Master of Science Thesis

Evaluation of the Elekta Synergy concept for patient positioning in image guided radiotherapy

Johan Renström

Supervisor: Per Nilsson, PhD and
Tommy Knöös, PhD

Medical Radiation Physics
Clinical Sciences, Lund
Lund University, 2005

Abstract

Introduction: The Elekta Synergy machine for external beam radiation therapy is equipped with an x-ray tube for on-line kV imaging and correction of the patient setup. The system can provide both 2D and 3D data for image guided radiotherapy (IGRT). Different aspects of the imaging system (called XVI) has been evaluated, such as image quality, flex of the gantry rotation, accuracy for patient setup correction, x-ray tube output and absorbed imaging doses.
Material and Methods: The stability in 2D and 3D image quality as well as the mechanical stability during rotation (also called flex) was measured on a weekly basis during a three month period. The stability of the system was studied by imaging a dense sphere positioned at isocenter. The 3D imaging was evaluated with a Catphan® 500 phantom and the 2D imaging with a Leeds phantom. Accuracy in patient setup corrections was evaluated by scanning a pelvis phantom in different locations. Readout from the software was compared to actual translational movements, which were defined by the room laser readouts on rulers mounted on the table-top in the x- y and z-direction. A gold marker matching study was performed using an Alderson/Rando phantom. Finally, both CT dose index (CTDI) and dose measurements with TLDs were performed. The TLDs were placed between the slices of the Alderson/Rando phantom using thin boards of polystyrene.
Results: The XVI showed minor long term variations in flex and stable image quality. The accuracy of detecting patient setup-errors based on bony structures was flawless, although matching with respect to gold markers failed. The received effective dose from a pelvis scan was about 11 mSv and for a head-and-neck scan about 0.15 mSv.
Conclusions: Even in its early commercial release the XVI system seems capable of detecting 3D setup-errors with a high accuracy. The software needs to be improved, however, to fully incorporate soft-tissue matching.

Contents

List of abbreviations

CBCT	Cone-beam Computed Tomography
CT	Computed Tomography
CTDI	Computed Tomography Dose Index
DICOM	Digital Imaging and Communications in Medicine
EPID	Electronic Portal Imaging Device
FOV	Field Of View
HVL	Half Value Layer
IGRT	Image Guided Radiotherapy
kV	Kilovoltage
kVp	Kilovolt potential
MPD	Multi Purpose Detector
MV	Megavoltage
MVCT	Megavoltage Computed Tomography
OMP	Oncentra Masterplan
PMMA	Polymethyl-methacrylate
PTV	Planning Target Volume
TF	Total Filtration
TLD	Thermo Luminescent Dosimeters
XVI	X-ray Volumetric Imaging Device
2-D	Two Dimensional
3-D	Three Dimensional

1. Introduction

1.1 Image guided radiotherapy

Today we know that radiotherapy is a prominent method for cancer treatment and it is widely used all over the world, often in combination with surgery. Physicists and engineers strive to optimize dose distributions and setup aids to minimize margins. These efforts tend to be a bit undone if there is a setup-error when positioning the patient on the table top. This error can be in the order of several millimetres. Therefore we must have further means to help minimize patient setup-errors. Today we have the technology that makes this possible, i.e. Image Guided Radiation Therapy (IGRT). IGRT uses different imaging devices to gather information about the patient setup prior to treatment delivery. If the patient is misplaced on the couch, then suitable corrections are made such that the patient can be treated as was decided during treatment-planning. When the patient is treatment-planned, a margin is added to the target volume (often several mm) which gives the planning target volume, PTV. The margin is added because of the requirement to kill all the clonogenic cells in the target volume with a high probability. The margin should be large enough to take care of setup-errors and target movement during treatment. Reduction of this margin, e.g. with the use of IGRT, would spare healthy tissue surrounding the tumour and can therefore significantly reduce complications that arise from the treatment. The complications are due to healthy tissue unnecessary being irradiated. IGRT can alternatively make it possible to increase the prescription dose to the tumour with the same level of complications [2]. This approach would increase the possibility to eradicate the tumour.

The IGRT technique started with the Electronic Portal Imaging Device (EPID), which uses the MV photons of the treatment beam to gather information about the patient setup. Initially not many portal imaging devices reached clinical acceptable performance regarding image quality [1]. It was not until the introduction of amorphous silicon flat-panel detectors that the acquired images could be used more reliably. But due to the high energy of the photons, EPID images still show very low contrast even with amorphous silicon flat-panel detectors. The images also have a low signal to noise ratio as the flat-panel detector can not be constructed to be efficient in detecting photons in this energy range. Therefore only tissues with high density (e.g. bone) are used in the matching process relative to the treatment planning CT images, which only enables coarse corrections of the patient setup [5]. Also imaging lungs can give satisfactory image contrast, even with MV photons, due to the high density difference between lungs (air) and soft tissue. Information about soft tissue movement is therefore lacking but highly needed in e.g. prostate treatments. Another disadvantage when using EPID-images is that they can only be acquired in planar mode and therefore matching can only be two-dimensional, unless EPID images are acquired at different gantry angles. The next step towards a more accurate matching

Figure 1.1 The EXACTRAC® X-RAY 6D IGRT system [26]. Two x-ray imaging devices give information about setup-errors.

process is to compare all the structures at hand and in all three dimensions. This is done on the Elekta Synergy radiotherapy unit, which incorporates a kV imaging system orthogonal to the MV treatment axis. Further information can be found in Section 1.3.

There are several ways to examine patient positioning using IGRT. Portal imaging with an EPID is the most common method but as technology advance new methods arise. When detectors become more efficient in detecting MV photons there are several possibilities for using the EPID detector when setting up the patient. One of them is the tomographic megavoltage technique (MVCT), which uses the same image reconstruction algorithms as in ordinary CT, but the projection images are those acquired with the MV imaging system. These systems are still under development [1,3] and there are no reports on this IGRT technology for routine clinical use. A portal imaging advancement that is widely used at clinics all over the world is based on the insertion of gold markers into the prostate when treating prostate cancer in radiation therapy. The EPID images acquired prior to treatment give both setup-errors based on bone tissues as well as soft tissue (prostate) movement by studying the translational movement of the gold markers. If an image is acquired orthogonal to the first one it is possible to receive information about approximate movement in all three dimensions.

Another approach of IGRT is to have two x-ray tubes directed at some angle (about140°) in relation to the gantry 0° origin position, one on each side, to image the patient position. One of those systems (installed at Rigshospitalet in Copenhagen) is called ExacTrac X-Ray 6D from BrainLAB IGRT, see Figure 1.1. Another type of IGRT system is based on an in-room CT positioned on rails. In this system the couch is shared between the CT and the radiation therapy unit, Figure 1.2. By using this approach the patient can be placed on the couch and imaged in the CT to examine setup displacements according to the dose plan. After correcting through a couch movement the patient can be treated in the right position, just by rearranging the couch to the same position in the radiation treatment machine reference frame.

Figure 1.2 The in-room CT on rails system. The couch is shared between a radiotherapy unit and a CT-scanner.

1.2 Cone-beam CT

Tomographic imaging can be performed in several ways. The most common way is to use fan beam x-rays and iterative reconstruction methods for the image reconstruction as in ordinary CT technology. A fan beam is narrow in the patient direction and to make a large volume scan the beam has to circle around the patient a number of times while moving the couch (or the imaging system). A cone-beam CT uses a beam which is wider in the patient longitudinal direction. This is illustrated in Figure 1.3. The broad beam property gives cone-beam CT an advantage compared to the ordinary fan-beam CT because it provides the possibility to make a whole volume scan in one single rotation. In a linac based system it would be practically unfeasible to use the fan-beam approach which implies that cone-beam imaging is demanded for these systems. This is mostly because of the time efficiency when using cone-beam CT but also because of the mechanical simplicity of the implementation. It is also important in cost comparison because it significantly reduces the workload on the x-ray tube [11]. But the cone-beam feature also has the disadvantage of elevated x-ray scatter reaching the detector at larger cone angles [2, 4]. The scatter problem gets even worse if the patient is large.

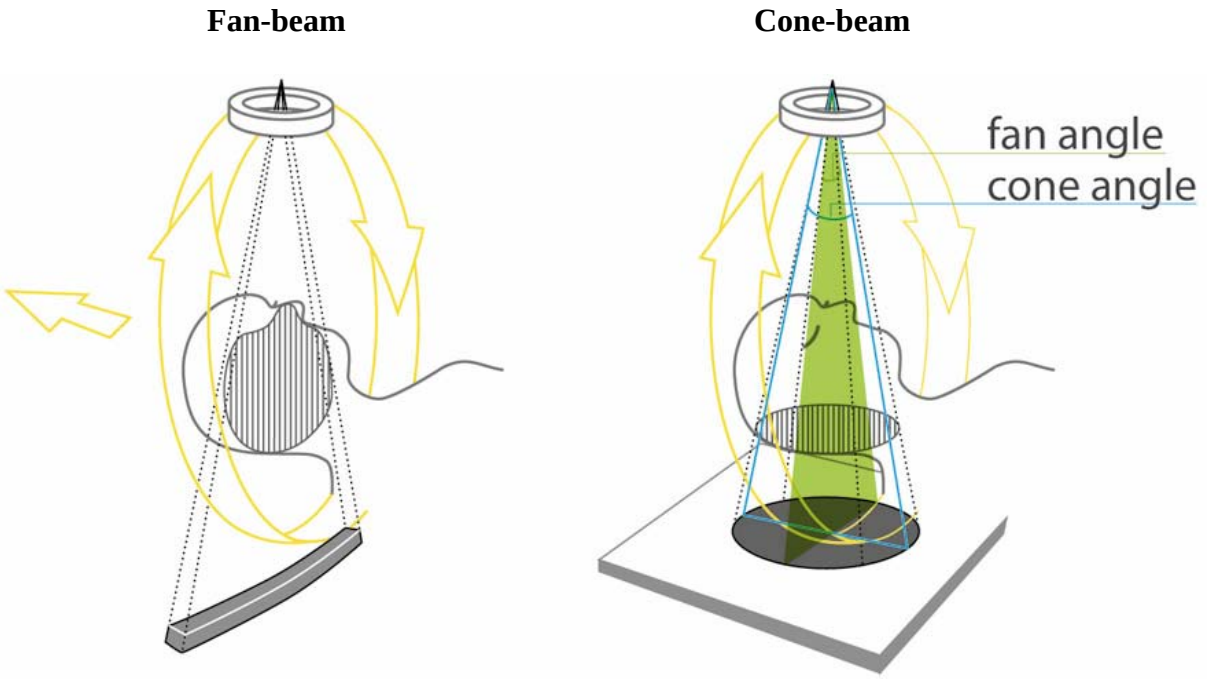

Figure 1.3 A schematic that shows the difference between fan-beam and cone-beam imaging. The cone-beam 2D-projections carry much more information than fan-beam projections. The scanned area in each projection is defined by the fan-angle and the cone-angle shown in the right image.

There are several ways to handle raw cone-beam data. The most widely used algorithm for image reconstruction is a Feldkamp-type algorithm [7,10], which is also the case for the XVI system. The Feldkamp-type algorithm uses an approximation in the Filtrated Back-Projection (FBP) process through a weighting function. The involved major parts of the algorithm include preweighting the projections, filtering and a 3-D backprojection. The weighting factor

compensate for the longer path that photons have to travel in the object at larger cone angles, i.e. for the increased attenuation [22]. The weighting is dependant on both the fan-angle and the cone-angle. The fan-angle defines the width of the beam across the patient in Figure 1.3 and the cone-angle defines the width of the beam in the patient direction. The algorithm handles discrete data which implies that the projection data needs to be sampled before reconstruction. Projections are handled row by row and the filtering is only implemented in the transverse direction of the sampled projections, for each row. Filtering is performed by using a so called ramp-filter for which the name originates from its appearance in the Fourier domain. Instead of a spatial convolution the filtering is performed through multiplication of the ramp-filter in the Fourier domain. The filter removes statistical noise in the Fourier space that otherwise would make the backprojection image appear smeared out. In the 3-D backprojection all filtered fan-beams projections have to be linearly interpolated along the tilted plane to determine the intensities in each voxel for a specific cone-angle. All these voxel intensities are then summarized to get the whole 3-D volume.

The Feldkamp-type algorithm is an approximate algorithm due to the weighting involved which causes off-midplane structures to be imaged inaccurately. This means that if large volumes are scanned, e.g. the pelvis, there may be artifacts near the edges of the image. Also, the increased path length for photons at higher cone angles gives rise to increased noise in the reconstructed images. The increased noise is due to the fact that less photons reach the detector if comparing to an ordinary fan-beam arrangement. The algorithm works sufficiently well in IGRT when there is a relatively long focal distance between the beam source and the detector, which causes the photon inclination to be almost parallel to the detector. It also has advantages compared to other algorithms including its simplicity and computational effectiveness together with the property to handle truncated data. The Feldkamp algorithm was first implemented in 1984 and of course there have been improvements since its original performance. Some examples are the P-FDK algorithm which rebins the data and makes a parallel beam reconstruction and the T-FDK which is capable of using more collimated beams for image reconstruction. The manual for the XVI [15] tells us no more than that the software uses a Feldkamp-type algorithm. Exact algorithms have been developed using noncircular orbits for image reconstruction but this feature would increase the complexity of the machine [8].

The mathematics of the Feldkamp-type algorithm is far beyond the scope of this work. Interested readers are referred to [6].

Altogether, cone-beam CT is a fast data acquisition technique which in its single circular trajectory scanning form demands little of the mechanical complexity on the machine. It can provide both the ability to image soft tissue in treatment position for an improved patient setup and the ability of monitoring patient movements during treatment delivery. One drawback may be that it puts more workload on the clinical planning and treatment process [1]. Imagine that there is a possibility to follow tumour growth or reduction during the treatment process. Then there is also a possibility to make new dose plans that fits the current tumour size, which would optimize the treatment process. This would not be possible in most hospitals, because it would demand unreasonable resources for each patient.

1.3 The Elekta Synergy machine

This thesis is about evaluating different aspects of the kV imaging system on the Elekta Synergy treatment unit installed at Lund University hospital. What makes this system special compared to other radiation therapy treatment units is its capability to image soft-tissue. This is done with an x-ray tube and an amorphous silicon (a-Si)/cesium iodide (CsI) radiation image detector panel [15] placed orthogonally to the treatment head and its EPID imaging device. This kV imaging system is called XVI by Elekta (X-ray Volumetric Imaging system). The XVI is sharing a common axis of rotation with the MV treatment source, Figure 1.4.

Figure 1.4 The Elekta Synergy machine. Image from reference [15, p 2-3]. The XVI system with its x-ray tube and x-ray detector is shown orthogonal to the treatment beam axis.

In a single 360 degree rotation, and sometimes even in a 180 degree rotation, the system can get a whole volume scan with slightly inferior image quality compared to a diagnostic CT-scan. During the 360 degree rotation the system will acquire approximately 650 planar images which are used to make a full three dimensional image, according to Section 1.2. The rotation takes approximately two minutes which unfortunately makes space for motion artifacts.

The kV photons are directed in a circular cone from the x-ray tube. The uncollimated cone has a diameter of 425 mm incident on the flat panel detector. Images can be acquired with three different Field Of Views (FOV); small, medium and large. The difference between the three FOV's is the offset from the kV central axis, which is 138.4 mm for the small FOV, 213.2 mm for the medium FOV and 262.0 mm for the large FOV. A schematic that shows the difference between a small and a large FOV is shown in Figure 1.5. When a FOV is chosen, the detector panel is shifted to match the beam offset via a translation in the up/down direction (if the gantry is set as in Figure 1.5). The nomenclature for the different directions related to the linac is shown in Figure 1.6. In the small FOV the beam is directed perpendicular incident on the detector, which means that the 138.4 mm offset is equal in both the "up" and "down" direction. When going to a larger FOV the beam is offset more, which in a circular movement of the kV imaging axis results in a wider volume being scanned. The cone diameter incident on the detector is the same for all FOV, 425 mm, but the beam differs in inclination with the choice of collimator.

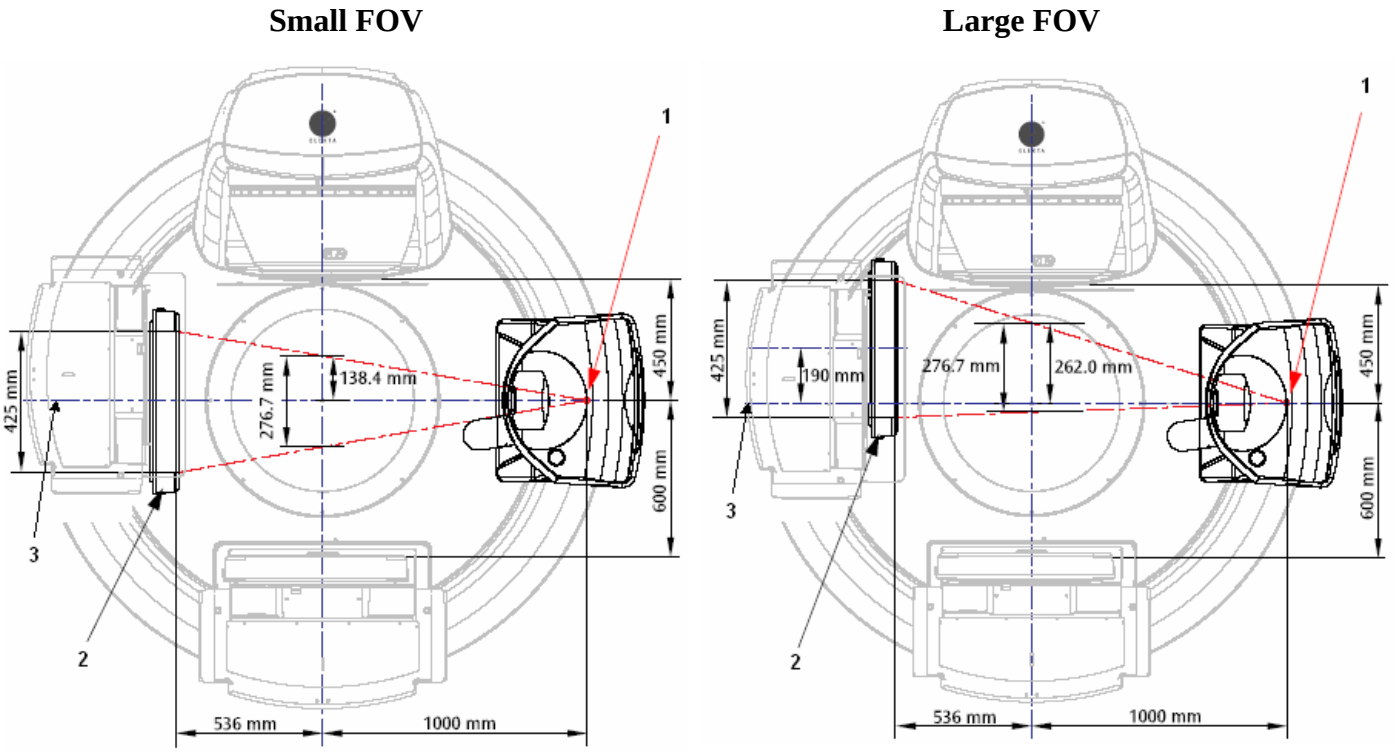

1. kV X-Ray beam focal spot
2. Image receptor (kV imaging panel)
3. kV X-Ray beam reference axis (*perpendicular to kV image receptor plane*)

Figure 1.5 A schematic of the Elekta Synergy arrangement viewed in the G-T direction with gantry at 0°. The small FOV arrangement is illustrated in the left image and the large FOV arrangement is illustrated in the right. It is shown that, when going towards a larger FOV, the beam is offset in the up direction. The detector offset from the kV-beam reference axis is shown in the right image, 190 mm. The beam offsets from the kV reference axis at isocenter are also shown, 138.4 mm and 263.0 mm, for small and large FOV respectively. Figures taken from reference [15, p 3-6].

For each FOV there is a collimator which is constructed to fit the specific FOV. The collimator consists of a cassette that can be inserted in front of the beam. An opening is defined by lead which collimates the beam. There are three different sizes of collimators for each FOV that collimates the beam in the G-T direction. The width of the beam in the G-T direction is called the “nominal irradiated length at isocenter” by Elekta and the values are shown in Table 1.1. The collimation in the Up-Down direction is the same for all collimators which means that the cone width is always 425 mm in the Up-Down direction incident on the detector (Figure 1.5).

Table 1.1 The different collimator cassettes for the Elekta Synergy kV imaging system. All cassettes produce a nominal irradiation field width (i.e. along the digital accelerator A-B axis) of 276.7 mm at isocenter. Table taken from reference [15, p 3-21]

Field of View	
Label	**meaning**
S	Small field of view
M	Medium field of view
L	Large field of view
Axial Field Length (Along digital accelerator G-T axis)	
Label	**Nominal irradiated length at isocenter**
2	35.16 mm (for medium FOV) 36.46 mm (for large FOV)
10	135.42 mm (for medium FOV) 143.23 mm (for large FOV)
20	276.7 mm

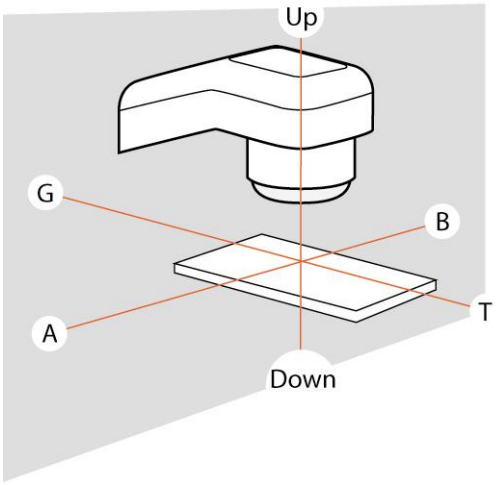

Figure 1.6 The nomenclature used for the different directions related to the linac.

Using the small FOV position enables volume reconstructions of up to 270 mm in diameter. When performing head-and-neck treatments or other treatments of less then 270 mm in diameter, it is preferable to use the small FOV. A medium FOV can construct images up to 410 mm in diameter, which is sufficient for a pelvis scan, implying that the large FOV is seldom (or never) used. The collimation in the G-T direction, using collimators marked **2**, **10**, or **20**, affects how large volume of the patient that is scanned. Changing the collimator is a way to reduce absorbed radiation doses given to the patient and at the same time reduce scatter that otherwise would affect image resolution negatively. Clinically the **M20** collimator is often used, but for example when scanning prostate it is sufficient to use the "thinner" **M10** collimator.

1.4 The XVI software

The most important part of the XVI system is the software installed for it. It handles for example communication with the hardware, algorithms for reconstruction of images and algorithms used in the matching procedures. It also is the graphical interface for which the user can interact with the system and if necessary adjust different parameters in it. Current version of the software used for the machine is "Release 3.5".

In this work matching procedures in the software is of major importance. After acquiring an image by performing an XVI-scan of the patient (for example when setup for treatment delivery), it is desirable to compare it to the treatment planned images. When the newly acquired image is moved a certain distance to fit the CT-images acquired for treatment planning it is called a matching. The matching in the XVI-software can be done in three ways. For clinical purposes the best way is to define a sub volume in the image using a clickbox tool and choose to let an algorithm do the matching for you, based on either matching for high densities within the clickbox or on a greyscale matching. The matching for high densities (called "Bone" matching) only takes into account tissue that has 1.5 times the density of

water. The greyscale matching does not use the clickbox. Instead all parts of the image are used in the matching, which naturally takes more time. The third way is to do the matching manually in all three dimensions, which is done when matching the ball bearing in the flexmap procedure (section 2.1.1).

For scientific purposes it is mostly desirable to be able to change the parameters of the predefined settings for each treatment, such that mAs, kV, and number of projections. The only way to set these parameters is to edit or create new presets in the software. Due to that the machine primarily is designed for clinical usage by nursing personnel, it was shown difficult to access and non-trivial to perform a change of the already defined presets. Changing the preset parameters is performed by reading a text file called “presetrules.ini” installed on the hard drive or by reading reference [18, Section 3.9.14]. In these documents can be found the rules for which parameters that can be chosen and how to define them. New presets are created by using those defined parameters while editing your own preset in another text file. The XVI software confirms if the defined preset is accepted and after that it can be chosen from the treatment-list.

The presets can also be used to define the voxelsize used for image reconstruction. It is possible to use a voxelsize between 0.1 - 10 mm. Clinically most presets use a voxelsize of at least 0.5 mm which demands about 300 projections to create. When images are imported to the XVI the software always converts image volumes into 256 slices, which means that the original CT-slices are not contained.

1.5 Flexmap theory

One of the most important checks on the XVI system in the Elekta Synergy machine is that the center of rotation is correct i.e. that the gantry rotates in a perfect circular trajectory. The deviation from perfect isocentric rotation is often called flex in this context. When displaying the flex as a function of the gantry angle a flexmap is obtained. Due to the weight of the accelerator head and the additional weight of the kV x-ray tube along with its flat panel detector, investigation of the flexmaps in the gantry rotation is required [12]. The weight causes perturbations in the circular scanning trajectory which give rise to flex that typically should be below 0.5 mm. Although this small shift seems like it can be neglected it produces a significant image distortion because of the short distance between the detector elements in the flat panel imager.

The flexmaps can be examined using a so called ball bearing phantom. The ball bearing phantom is much like a perfectly spherical dense ball placed at the end of a long Perspex rod. The phantom can be attached to the table top and adjusted by vernier screws in all three dimensions, see Figure 1.7.

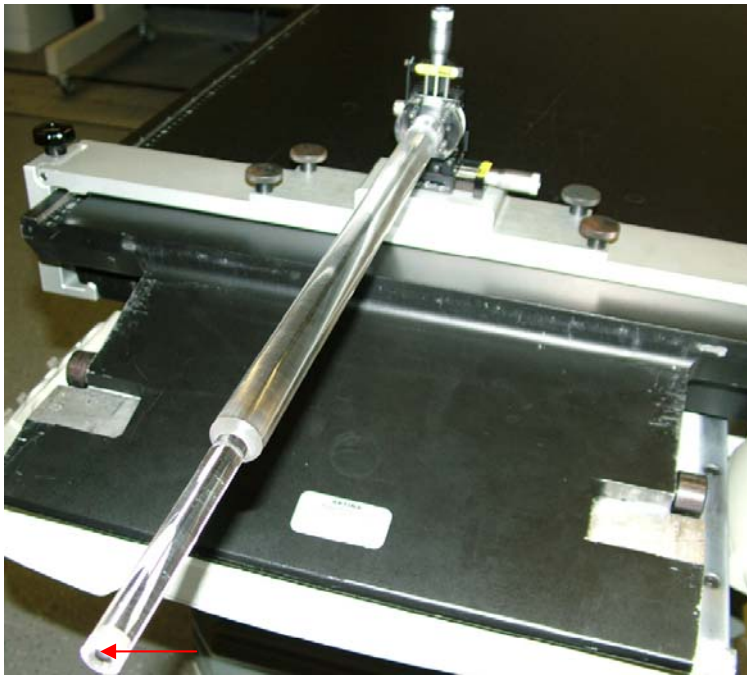

Figure 1.7 The setup of a ball-bearing phantom. It is placed where the removable table top normally is inserted. The red marker shows the location of the dense ball.

With this setup a number of projections are made while the gantry rotates in a circular trajectory. The projection of the ball bearing positioned at isocenter shows the amount of shift at different gantry-angles. The ball bearing phantom can be used to calculate both the kV and MV imaging systems shifts from isocentric rotation. It is important to examine the difference between the kV flex and the MV flex since the MV imaging system is used to setup the ball bearing in isocenter. Still, it is not possible to align the ball-bearing phantom perfectly in isocenter and therefore it is needed to subtract the non-correctable MV flex from the kV flex. This way a correct kV flexmap is acquired which is less dependant on a correct setup. More information on the flexmap procedure can be found in Section 2.1.1.

The XVI software supports image calibration that considers the flex. For each projection during image reconstruction, the data is shifted according to the flex for the specific projection angle. The flex is gathered from a stored lookup table that has been implemented by using the full flexmap calibration in the software. The full flexmap calibration is performed as an additional step in the flexmap procedure described in Section 2.1.1.

2. Material and methods

2.1 Continuous quality assurance and acceptance tests

Like all machines that produce ionizing radiation given to patients, Quality Assurance (QA) periodic tests have to be done. The ordinary periodic tests of the treatment accelerator are performed on a weekly basis. According to [1] the experience so far with integrated kV imaging systems mounted on the radiation therapy unit, quality assurance tests should be done with the same frequency as on a conventional accelerator or a simulator. Therefore two types of quality assurance tests, related to the XVI-system, are done on a weekly basis. The first one is a test that investigates deviations from isocentric rotation of the gantry and the other is an ordinary image quality test of the generated images. Both tests are described in more detail in the sections below.

2.1.1 Flexmap and isocenter checks

A part of this thesis is to investigate the difference in flex relative to isocenter between the kV and MV imaging systems on a weekly basis and correct for possible disorders that exceeds 0.5 mm in successive measurements. The correction will in that case be a recalibration resulting in a new flexmap. The procedure is done completely in the software. A ball bearing phantom, described in Section 1.5, was used when evaluating the flexmap. The instructions for the procedure can be found in reference [17, Section 8.7]. A short summary of the elements included in the procedure follows below. First the MV-photons from the linac are used to image the dense ball, positioned at isocenter, with the IviewGT (Elekta's EPID-device) at gantry angles 0°, -90°, 90° and 180°. Also, another four images need to be acquired, one for each of the four gantry angle mentioned above, but with the collimator rotated 180°. The IviewGT data are then exported to the XVI software, for which the procedure also can be found in reference [17, section 8.7]. From these imported data, the XVI software calculates the isocenter with respect to the collimated beams in each of the directions. The software also displays how much the location of the dense ball deviates from isocenter. If the location of the ball is off by more than 0.25 mm relative to the isocenter in any direction, it is adjusted with the three vernier screws described in Section 1.5. After the adjustment new MV-images are exposed, from which another check is made that the ball bearing is off by no more than 0.25 mm from isocenter. This procedure has to be repeated until the demand is fulfilled. The MV image flex from the isocenter is then registered. Figure 2.1 shows a screen dump from the XVI software.

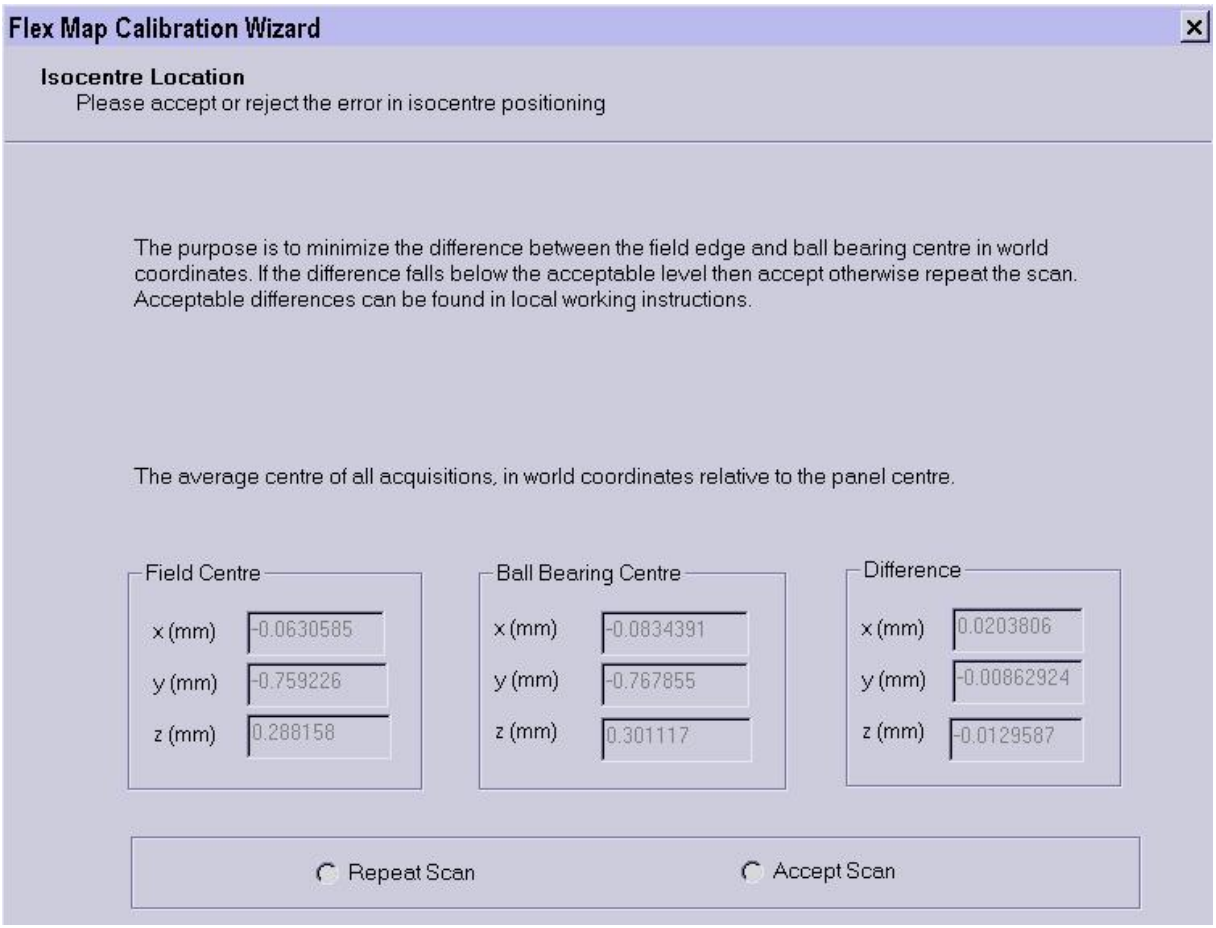

Figure 2.1 A screen dump from the full flexmap calibration wizard in the XVI software. The "Field Centre" column is calculated from the collimated MeV beams taken at eight specific positions. It shows the average position of the MeV beam isocenters. The "Ball Bearing Centre" column shows the average position of the dense ball for those eight beam positions. Subtracting the ball bearing column from the field center column results in the "Difference" column, which shows the position difference between the beam isocenter and the center of the dense ball.

After this process the kV flexmap check is initiated. The procedure for this can be found in reference [16, Section 2.10]. In short a volume view image is constructed and matched against a dummy ball which is created by the program at isocenter. Figure 2.2 shows a screen dump that illustrates how the matching is done. The purple area (plan) is moved manually in all three directions such that it is fitted as good as possible compared to the newly acquired image of the dense ball (green area). The values recorded for the kV flex are those shown as "Table correction". The difference between MV and kV isocenters is calculated and tabulated.

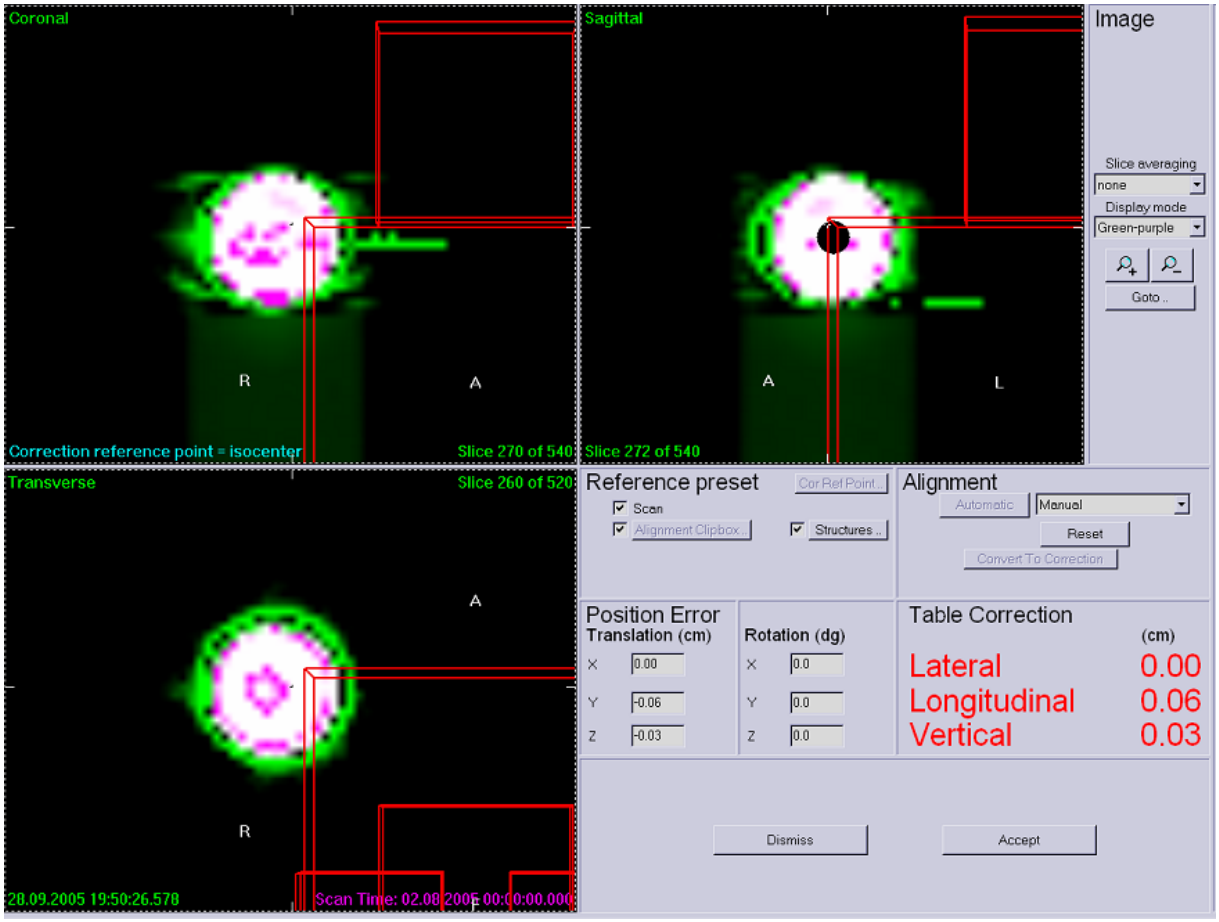

Figure 2.2 The correction window in the XVI software. The images show the shift of the ball compared to the isocenter. The green area is the acquired volumetric image and the purple area is from the dummy ball placed at isocenter (plan). A manual matching has been performed by moving the plan in coincidence with the green acquired image prior to the screenshot. The red lines on the right side in each view are to illustrate the view directions in the software and they have nothing to do with the matching.

When calculating the difference between the kV and MV flex from isocenters, those values displayed under “Table correction” have to be direction inverted because the program displays suggested couch movements and not position errors (actually the program displays both but it is only those displayed as “Table correction” that have been converted into translational couch movement from possible rotations in the setup).

2.1.2 Imaging tests, 3-D and 2-D

All imaging tests are performed according to reference [16, section 2.8-2.9] and as with the flexmap test they are done on a weekly basis. The 3-D imaging tests are carried out using a Catphan® 500 phantom which is designed for comprehensive evaluation of axial, spiral and multislice CT scanners. Figure 2.3 shows a picture of the phantom. The phantom has a number of compartments for analyzing different image quality properties. Figure 2.5 show a schematic of the phantom.

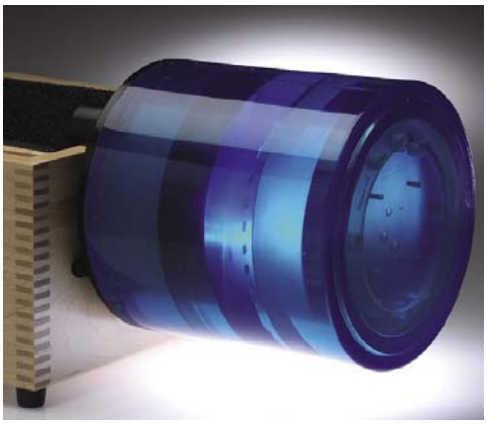

Figure 2.3 The Catphan® 500 [19]

The 3-D imaging tests are performed by scanning the Catphan® 500 in a volume view reconstruction, using the predefined preset “CAT – Image Quality”. The phantom is placed on the table-top and aligned according to the protocol.

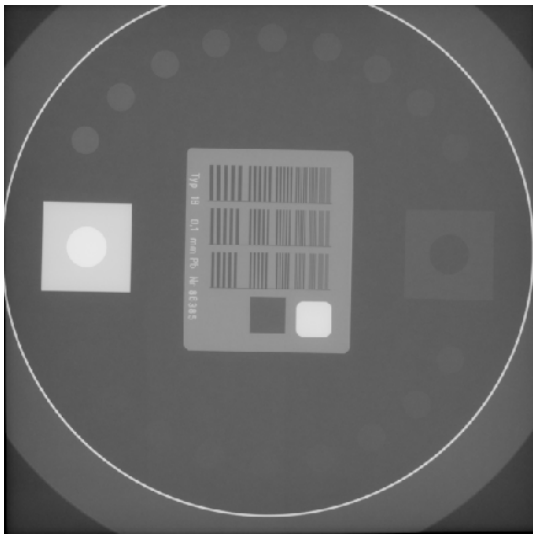

Figure 2.4 A planar image of the TOR 18FG Leeds Phantom. Low contrast discs are located peripheral in the phantom and the spatial resolution module is located in the centre.

The quality assurance protocol is determined to evaluate 3D- and 2D low contrast visibility, 3D geometric accuracy, 2D- and 3D spatial resolution and finally 3D uniformity. The contrast is a measure of the difference in displayed brightness between the lightest and the darkest pixels in an image. A problem in cone-beam reconstructed images is the increased noise, as mentioned in section 1.2. The 3D uniformity is a way to measure image noise by comparing pixel values in a homogenous material. Low-contrast visibility is the resolution of a low-contrast object and it is influenced by several factors, including image noise, object size and contrast between object and background. Therefore it is important to analyze the low contrast visibility. The spatial resolution determines at what extent small structures can be separated in the image. This is of major importance when it is needed to detect small objects in the image.

The low contrast visibility is evaluated by investigating the mean pixel values together with the standard deviation for two different subcompartments with known density in the phantom. The 3-D spatial resolution is analyzed at the location of the spatial resolution module in the phantom, by determining how many line pairs that can be resolved. The last 3-D imaging test is to examine the uniformity module of the phantom. Four different mean pixel values are retrieved at random parts in the image and the percentage difference between the maximum and minimum value is recorded.

Also a measurement is performed that determines if the transverse vertical and horisontal length across the inserts are 117 mm in the software measurement utility, i.e. the true physical distance. Also the sagittal geometric accuracy is determined by measuring the distance between two marked points in the sagittal view.

The 2-D imaging tests are performed using a TOR 18FG Leeds Phantom placed on the carbon fiber table top at isocenter. A PlanarView^{TM} (planar) image is acquired using the “Panel Alignment – Small FOV” preset and the gantry angle at -90°. There are sections in the phantom for analyzing contrast and spatial resolution, according to Figure 2.4. The low contrast is analyzed by counting the number of visible low contrast discs. The spatial resolution is analyzed by counting the number of spatial frequency groups where the line pairs can be separated.

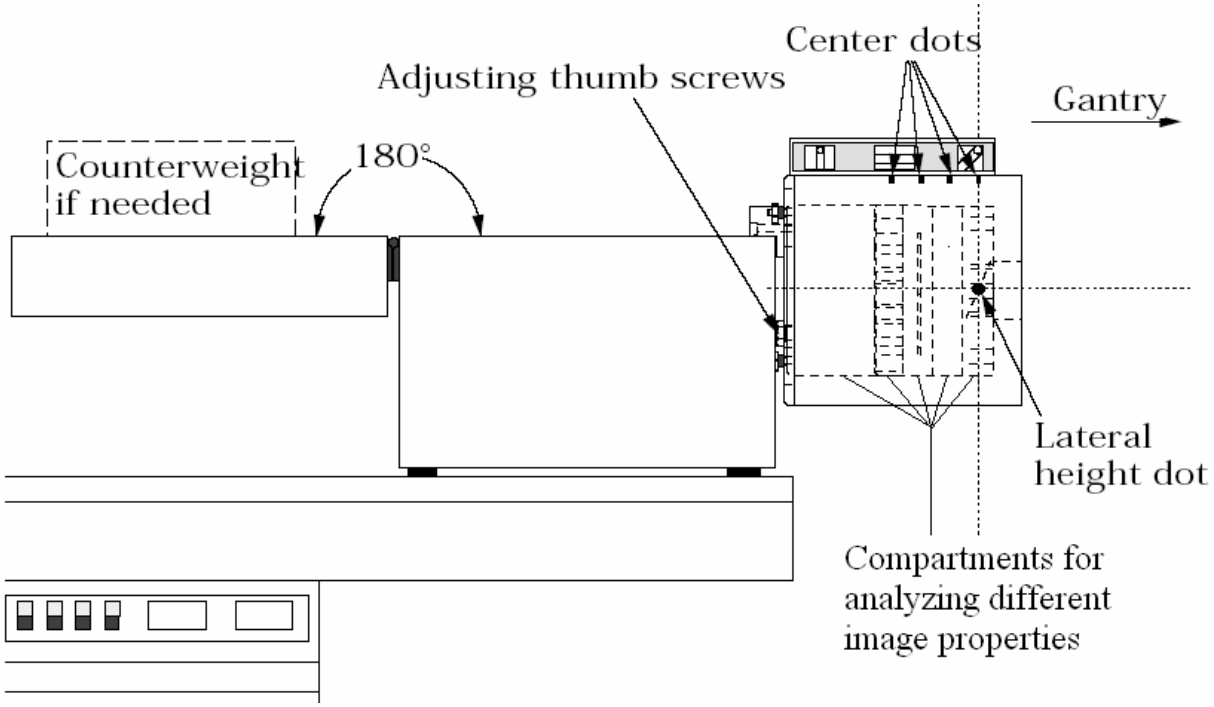

Figure 2.5 A schematic of the The Catphan® 500 phantom [19]. It is shown how the phantom is positioned on the table top and how the different compartments are organized in the phantom. Dots painted on the phantom helps to position it at isocenter and the adjusting thumb screws are used to level the phantom correctly.

2.2 Detection limits of the system

The Elekta Synergy product is very new to the market and has therefore not been extensively evaluated by a number of sites. Here at Lund University Hospital the XVI is so far sparsely used for patient positioning but the nurses develop protocols of data for comparing EPID and XVI matches on a daily basis. In this thesis phantom studies were performed to investigate the matter. Most interesting to study is whether the XVI system can detect the setup-error, by performing a scan and a matching procedure, when a phantom has been moved a well defined distance from the treatment planned position. This part will be discussed in detail in section 2.2.1. Also, clinical usage of the XVI has reported that there seems to be problems when matching with respect to gold markers placed in the prostate. Therefore this was evaluated by placing gold markers into the Alderson/Rando phantom and setup-error recognition was then tested in the XVI. More information on this matter follows in section 2.2.2.

2.2.1 Pelvis phantom study

For some reason images acquired in the XVI cannot be set as reference images. Instead it is required to perform a CT scan after which the DICOM images are exported to the XVI. Due to this we began to scan a pelvis phantom designed by “The phantom laboratory” of the type “Sectional Pelvis real bone phantom” (76-642-3000) in our CT-scanner (General Electric HiSpeed NX/i Pro) with 3 mm slices. The scan was performed with the phantom placed in its fixation device to facilitate positioning. After the CT images were processed in our treatment planning system (Oncentra MasterPlan (OMP) from Nucletron) they were exported to the XVI-system. If there is no treatment plan set, the images cannot be imported as reference

images by the XVI software. After planning in OMP a physicist aligned a matching volume in the reference image imported. The same matching volume was used to match all images taken further on, so that this parameter would not affect the precision of the matching. All matchings were carried out using a “Bone” automatic matching in the software. According to [5] the most accurate matching was found to be when making a manual match in the XVI. Although, from the much increased workload to hospital personnel when performing a manual match, it follows that this is not considered to be an option.

It was decided to define the actual translational movements of the phantom to be related to the room lasers. Rulers with mm precision were created that easily could be attached to the couch in the treatment room. The subjective thickness of the laser lines on the rulers were exactly 2 mm across which resulted in excellent precision when letting the centre of the laser be aligned over the defined value (both edges of the laser was then in line with marked millimetres on the rulers). Also, the displayed couch movement on the treatment room monitors have mm precision, but these values are discrete and can therefore not be as precise as the reading of the laser lines on the rulers. The displayed couch movement was only used to double-check our measured laser movement. Figure 2.6 shows the setup of the study.

Figure 2.6 The setup of the detection limit measurement. The left image shows how the pelvis phantom and the rulers are placed on the couch. It is shown how the rulers can define movement in the x- y and z direction. The right image shows a closer view of the rulers and how we get readouts with mm precision from the lasers.

Different examination protocols have predefined presets as they are called in the XVI software. The presets handle x-ray tube output, choice of collimator, number of projections, etc. As shown in Figure 2.6, the phantom was set up on the couch and aligned at isocenter according to the room lasers. It was scanned by the XVI with the “Pelvis” preset, which uses a **M20** collimator for a broad scan. This image is called the second reference image. The suggested couch movements when matching the second reference image against the CT image (reference image) were stored. Instead of trying to correct for these small discrepancies by adjusting the couch position, only relative translations are measured. This means that the suggested couch movement, when matching the second reference image to the first, was subtracted from each of the displayed setup-errors in the rest of the study.
It is desirable to evaluate at which accuracy the software can detect translational movements in all three dimensions. Therefore the phantom was moved 2, 4, and 8 mm in each of the six

possible directions, A, B, G, T, Up and Down, respectively (Figure 1.6). A scan is performed after each translation and the automatic matching relative to the CT reference images displays the suggested couch movements. The same procedure was repeated while moving the phantom 2, 4, and 8 mm, equal distance in all three possible directions simultaneously. This process makes it possible to evaluate the accuracy of 3-D movement detection in the software and also how accurate it converts the 3-D movement to 1-D translations in each direction. The software is also constructed to register rotations of the patient, but if the unit installed does not support couch rotations, the software translates rotations to translational movement in all three directions. Finally one scan was made moving the phantom 2 mm in B direction, 4 mm in Down direction and 8 mm in T-direction, to test the accuracy of irregular movement detection.

2.2.2 Alderson/Rando phantom study with inserted gold markers

The Alderson/Rando phantom is a whole body phantom (except for arms and legs), consisting of 2.5 cm thick slices, as shown in Figure 2.7. It is primarily used for dosimetric purposes, which is the case in Section 2.4.2, but it is also well suited for this measurement. There are pre-drilled holes in the Alderson/Rando phantom slices which are normally used for insertion of TLDs. Tissue equivalent plugs were manufactured, where the gold markers are glued to the inside of small drilled tracks. The gold markers are 5 mm long and have a diameter of 1 mm. By placing the marker on top of each plug the markers can be separated in the axial direction of the phantom by inserting the plug in different directions. The gold markers are usually placed about 20-25 mm apart when inserted into a real prostate patient. Using the pre-drilled holes in the phantom, the best possible arrangement is chosen for positioning the gold markers so that it mimics a real prostate marker implant. It is also preferable that the markers are not in the same dimensional plane and that they are orientated in the phantom to where the prostate would have been located, considering the phantom appearance. Slice 30-35 of the Alderson/Rando phantom is used for the insertion of the gold markers. Two plugs with markers are inserted into slice 34 with the markers in the cranial and caudal part of the slice, respectively. These markers are also separated in the x-y direction. The third marker is placed in slice 35, which is caudal of slice 34, with the gold marker in the cranial part of the slice.

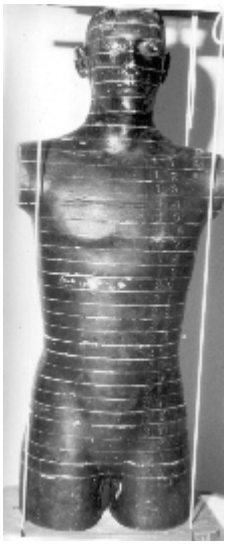

Figure 2.7 The sliced up Alderson/Rando phantom. [27]

A CT scan of the Alderson/Rando phantom, with the gold markers inserted, was performed prior to the measurement. The scan was carried out on a Siemens Somatom Sensation Open CT-scanner, using 3 mm slices. Also a treatment plan was made in OMP, to be able to send the images to the XVI. The images are then imported into the XVI software and accepted as reference images. In the reference image a matching box is added that covers all three gold markers, but no bony structures. In this way it is evaluated at what accuracy the XVI software can detect prostate motions through a matching with respect to the gold markers alone, and not with respect to bone tissue.

2.3 X-ray tube performance

All x-ray equipment in a hospital has to be tested regularly following a quality assurance protocol. This also includes the XVI imaging system. The test includes examining whether the kV and mAs output from the x-ray source coincide with the settings in the preset of the software. Another important characteristic to be examined is whether the dose increases linearly with mAs. It is also checked if the filtration thickness tabulated in reference [18, Section 3.3.1.1] coincides with measurements. A “Panel Alignment - Small FOV” predefined preset was used and adjusted to fit the measurement. How presets are defined was described in section 1.4. For some reason only two different kV settings could be used, 100 kV and 120 kV, although the manual says that kV values between 70-150 kV can be set. The mAs could be varied in specified steps according to the “presetrules.ini” file and it is divided up as “nominalmsperframe” and “nominalmAperframe”. The “nominalmAperframe” parameter was varied when setting the mAs and the “nominalmsperframe” was held constant at 25, with a number of 15 frames in all measurements. The mAs is calculated by the software and shown in a dialogue window when choosing the preset.

An RTI Electronics, Barracuda system is used for the tests. It consists of a Barracuda MPD detector along with its power unit/electrometer and a Palm Tungsten T3 handheld computer. The MPD detector (Multi-Purpose Detector) measures kVp, time, pulses, dose, dose rate, dose per pulse, pulse rate, HVL, total filtration and waveforms, all in one measurement. The Palm has a dedicated “QA browser” software installed, which handles communication with the detector and displays the output. The MPD detector is placed at isocenter (SSD = 100 cm). The Palm was placed as far as possible from the x-ray beam on the couch.

2.4 X-ray imaging doses

There are regulations for clinical usage of ionizing radiation for diagnostic purposes. Even though the XVI is mounted on a therapy unit it must be categorized as a diagnostic device. Therefore it is desirable to examine the acquired doses when performing XVI scans prior to treatment. In this thesis two different approaches are used to evaluate absorbed doses, Computed Tomography Dose Index (CTDI) and absolute measurements using Thermo Luminescent Dosimeters (TLD).

2.4.1 CTDI-measurements

CTDI studies are primarily designed for evaluating doses using a fan-beam geometry but this difference should not affect the results more than other possible perturbations described in Appendix A. For determination of CTDI, a phantom designated for CTDI measurements is used [4]. It consists of two circular PMMA blocks with drilled holes for inserting the ion chamber. The blocks are constructed such that the smaller one can be placed inside the bigger one. In this way it is possible to have either a block with 16 cm diameter or when both blocks are mounted the diameter is 32 cm. The phantom is placed on the table top in its bracket and aligned at isocenter using the room lasers. As described in Appendix A it is required to measure the doses in the center of the phantom and in four peripheral points. In the center at

least three measurements are required to give an acceptable mean value. The peripheral value is calculated as the mean dose at four different angles. The phantom used here at Lund University hospital could not measure at 180° which forced us to make the measurements in the following angles instead, -45°, 45°, -135° and 135°. Measurements in these positions should give the same results as if we still have measured four points orthogonal on the circular phantom.

In the XVI software there are predefined presets for different examinations. For the 32 cm diameter phantom, a Pelvis preset is chosen, which uses 120 kV as tube voltage and 650 mAs. The doses are measured with a Radcal Corporation 9010 Radiation Monitor controller and a 90X6-3CT ion chamber with preamplifier. Two different collimators are used in the measurements, **M10** and **M20**.

For the smaller phantom, which is 16 cm in diameter, a head-and-neck preset is used in the XVI software. This preset uses a **S20** collimator, 100 kV tube voltage and 36.1 mAs. In this case several measurements have to be done in the peripheral points due to that the gantry does not make a full 360° rotation in a head and neck treatment. The dose in each angle will be very different and it is not sufficiently accurate to use the mean of only one value at each angle. The gantry makes a 180° rotation in the head-and-neck preset.

2.4.2 TLD-measurements using an Alderson/Rando phantom

2.4.2.1 Pelvis

TLD-measurements using an Alderson/Rando phantom should also give an estimation of the received patient dose in a XVI-scan. Each of the Alderson/Rando slices has drilled holes for inserting optional rods, in which two thermoluminescence detectors, TLD's, can be placed. If the rods are not inserted, they are filled with tissue equivalent plugs. The holes are drilled in soft tissue only. Because of a shortage of TLD rods another approach was used in the measurement. Thin boards of polystyrene with small rectangular holes for TLDs, which can be placed between the slices of the Alderson/Rando phantom, were used. Figure 2.8 shows how the boards are placed between the slices in the Alderson/Rando phantom.

Figure 2.8 The arrangement of the TLD insertion in the Alderson phantom. Thin PMMA boards with square holes are placed between the Alderson/Rando slices. The TLDs are placed in these holes.

We used TLDs of the fabricat Harshaw TLD100 LiF which have the dimensions $3\times3\times1\,\mathrm{mm}$. Before inserted in the phantom the TLDs are warmed up to empty shallow traps. The TLDs are then positioned in the phantom at various positions, which should represent both the deep and peripheral positions in each of the three Alderson slices. Two groups with 20 TLD's in each group are used in the measurement. From these 40, two TLDs in each group are used for constancy checks and two for background subtraction. This means that we have 32 TLDs for the in-phantom measurements. The two TLDs for constancy check are irradiated to a well defined dose using a ^{60}Co -source. Their acquired doses are given as input to the TLD readout program, together with the background dose.

Figure 2.9 The Alderson/Rando phantom assembled and with the TLD's inserted

For the pelvis measurement, after placing the TLDs, the phantom is put assembled using a mechanism according to Figure 2.9. The phantom is then placed on the couch at isocenter with the G-T laser aligned at the center of slice 32 in the Alderson phantom (exactly in between the two polystyrene boards). A pelvis preset is used for the XVI scan, i.e. the **M20** collimator is used with a medium FOV. As in section 2.4.1 the preset uses 120 kV and 650 mAs.

2.4.2.2 Head and neck

The same procedure as described in Section 2.4.2.1 is performed for a head-and-neck measurement. This time a head-and-neck preset is chosen in the XVI, which uses a **S20** collimator and a small FOV. For a head-and-neck treatment, tube voltage is set to 100 kV and 36.1 mAs. In this case there were five polystyrene boards for a complete coverage of the head-and-neck area. Like in the TLD measurement of the pelvis there were 32 TLDs to measure with, which resulted in that all holes could not be filled. Instead the TLDs were placed at locations that best covered the whole head-and-neck region. Four of the 32 TLDs were placed in the eyes, two in each eye, to measure the eye doses. The phantom is placed in isocenter according to the room lasers, with the G-T laser aligned at the center of the board between slice 5 and 6. A head-and-neck scan is made in a 180° rotation.

3. Results and discussion

3.1 Mechanical stability – flex evaluation

The flexmap procedure described in Section 2.1.1 was carried out at eleven separate occasions with about one week interval. A crucial part to evaluate is the difference between the MV and kV imaging systems isocenter deviation (flex). The flex differences received during those eleven occasions, displayed for each of the three directions, is shown in Figure 3.1.

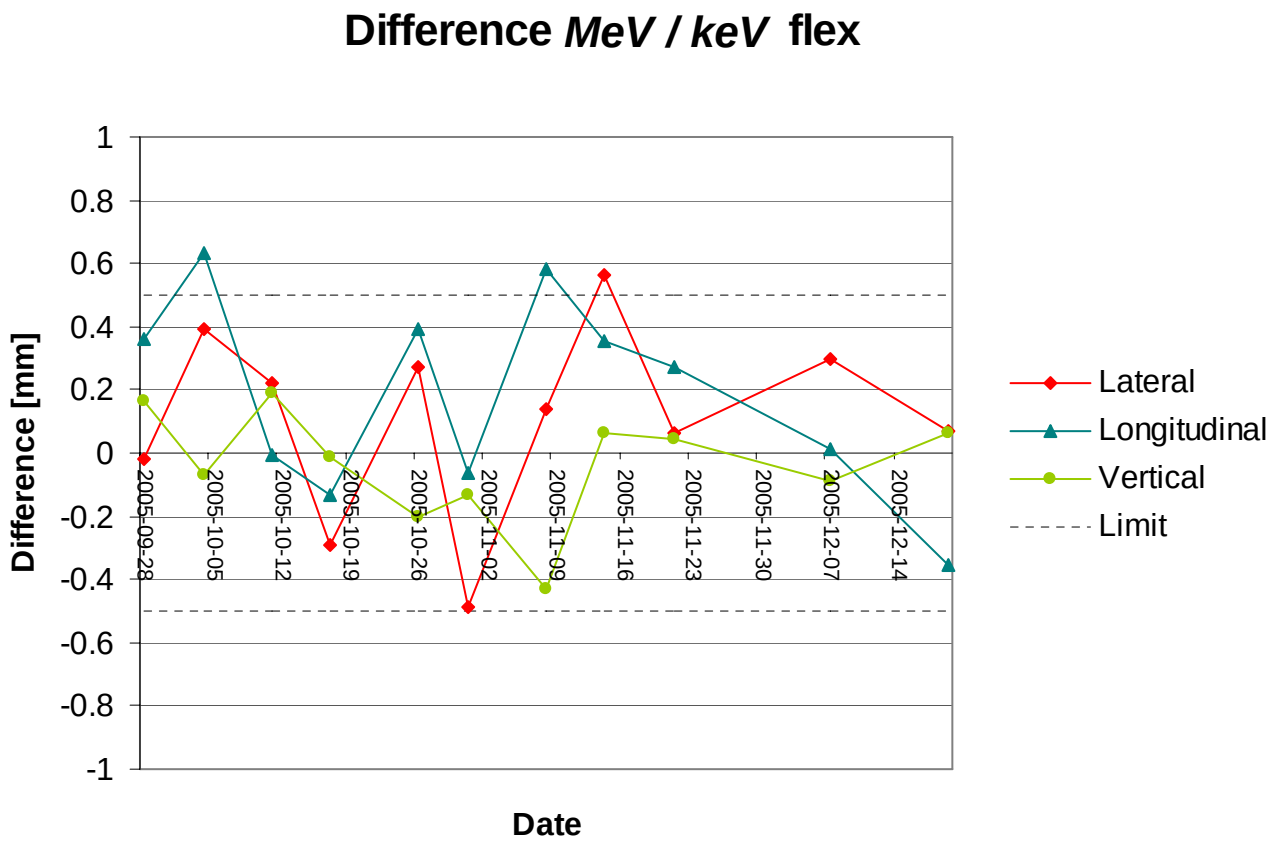

Figure 3.1 Difference between kV and MV imaging system's flex at different occasions, shown for all three directions. Dashed lines indicate limits set by the manufacturer.

As seen in Figure 3.1, the results show relatively small variations in the flex from date to date. Three occasions show a flex difference greater than the tolerated limits. Due to the fact that the Elekta Synergy system is new on the market there is limited knowledge of the accuracy of the described flexmap procedure and its results. This, together with the fact that there were no successive measurements outside the limit of 0.5 mm, resulted in that no flexmap recalibration was made during the eleven week test period.

If analyzing uncertainty factors involved in the flexmap procedure the largest errors arise from the matching procedure (Figure 2.2). Moving the acquired image of the dense ball one

pixel relative to the plan, can result in a difference of the kV flex by 0.1 mm. It is not obvious when the image is centred over the plan which means that there may be about 0.2 mm errors only in the kV flex. Figure 3.1 shows that a 0.2 mm error would change the flexmap appearance considerably. The errors in the MV flex are more difficult to estimate due to the fact that it is hidden in the software.

3.2 Acceptance test results and their long term stability

Successive measurements according to Section 2.1.2 has been performed at ten different occasions during a three month period. The purpose of the tests is to examine different image properties of the XVI system and to evaluate the stability of the system during the three month period. The first property that is examined is the 3-D Low-contrast visibility. Figure 3.2 shows the variation of 3-D Low-contrast as a function of time.

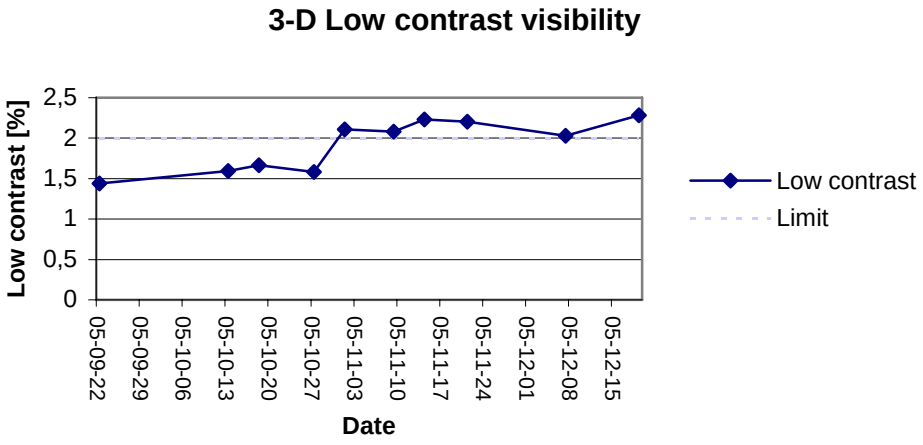

Figure 3.2 The measured 3-D Low contrast visibility at ten different occasions during a three month period. The dashed line show the 2% limit set by Elekta.

As can be seen a possible trend is that the 3-D Low-contrast visibility slowly deteriorates. More than half of the measurements show 3-D Low-contrast visibility that does not fulfil the 2% limit set by the manufacturer. The result has been reported to Elekta and they responded that they are aware of it. The problem arises from a bug in the software that will be fixed in the next version.

Also deviations between measured distances with the XVI software and actual distances in the Catphan phantom have been evaluated. The results showed that the system seems stable in this matter and that all measurements were within tolerances, Table 3.1.

Table 3.1 The deviations between distances measured with the XVI software and actual distances in the phantom. The mean is calculated for all ten occasions.

Direction	Mean deviation [mm]	Maximum deviation [mm]
Lateral	0.48	1.04
Longitudinal	0.40	1.04
Vertical	0.67	1.04

The mean value of the measured 3-D Uniformity during the three month period was 0.67% which is well below the set 2% limit. There seemed to be no trends in consecutive measurements. The same applies to the 2-D Low-contrast visibility and the 2-D Spatial resolution measurements. The mean for the 2-D Low-contrast visibility was 2.13% where the tolerance is 3%.

Spatial resolution is a measure of how many line pairs that can be resolved per mm. Calculated 2D-spatial resolution mean value of the ten occasions was 1.8 lp/mm which is better than the limit value of 1.4 lp/mm. The 3-D spatial resolution has been very stable over time but it also has been close to not fulfilling the threshold value. 0.7 lp/mm was recorded in almost every measurement and that is also the demanded limit by Elekta. The results are summarized in Table 3.2.

Table 3.2 Different image properties of the XVI system resulting from the acceptance tests carried out at ten different occasions

Image property	Measured mean value	Tolerance value set by Elekta
3-D Uniformity	0.67%	$\leq 2\%$
3-D Spatial resolution	0.7 lp/mm	≥ 0.7 lp/mm
2-D Low contrast visibility	2.13%	$\leq 3\%$
2-D Spatial resolution	1.8 lp/mm	≥ 1.4 lp/mm

3.3 Detection limits of the system

3.3.1 Pelvis phantom study

An interesting feature to look into is whether the system detects and accurately corrects for translational set-up errors. The results of this test are presented as the difference of deliberate movements in relation to the lasers and the XVI suggested setup-error, as a function of the moved distance. Figure 3.3 shows a plot where difference between actual phantom movements defined by the lasers and XVI suggested movement back to origin, is plotted against the phantom movements defined by lasers.

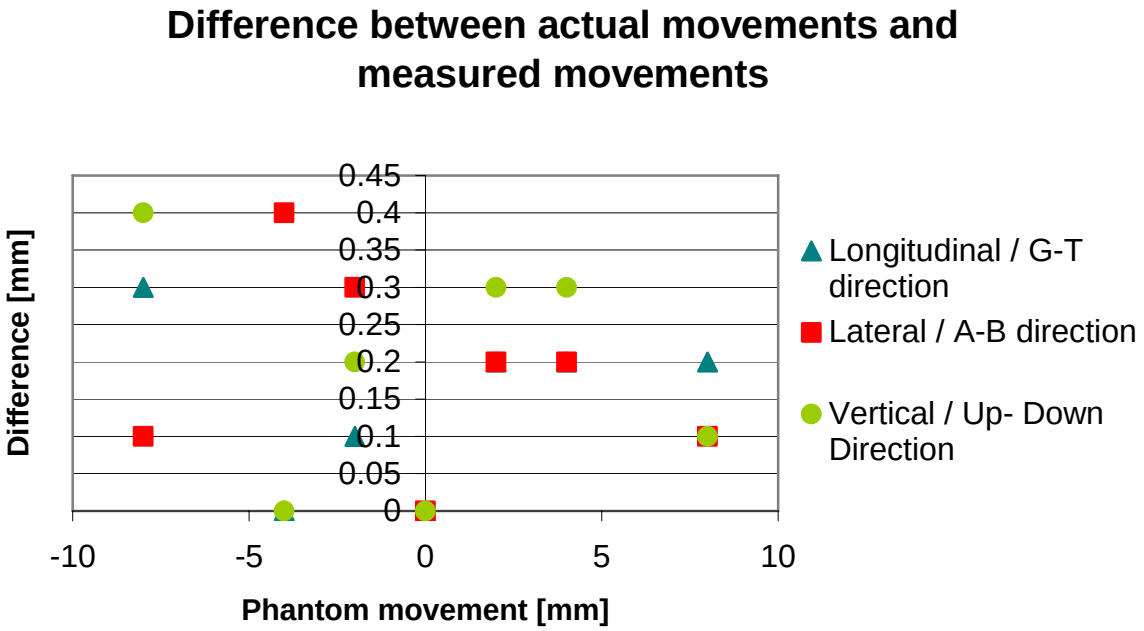

Figure 3.3 The measured difference between translational movement of the phantom according to the room lasers and the translational movement according to the XVI software.

An alternative presentation of the data is shown in Figure 3.4. It shows a more perspicuous schematic of the amount of relative difference between the “actual” phantom movement according to the lasers and the different XVI suggested movements. The area for each colour gives a rough idea of how much the software fail to register translations in each direction. It could intuitively be expected that the software showed increased correction deviations when the phantom was moved a larger distance but no such tendency can be seen. Instead, the combined Figure 3.3 and Figure 3.4 shows that the XVI software seems to correct our deliberate phantom movements with very good accuracy. The maximum deviation found was 0.4 mm, which could equally well depend on setup-errors of the phantom relative to the lasers as it would depend on errors in the software.

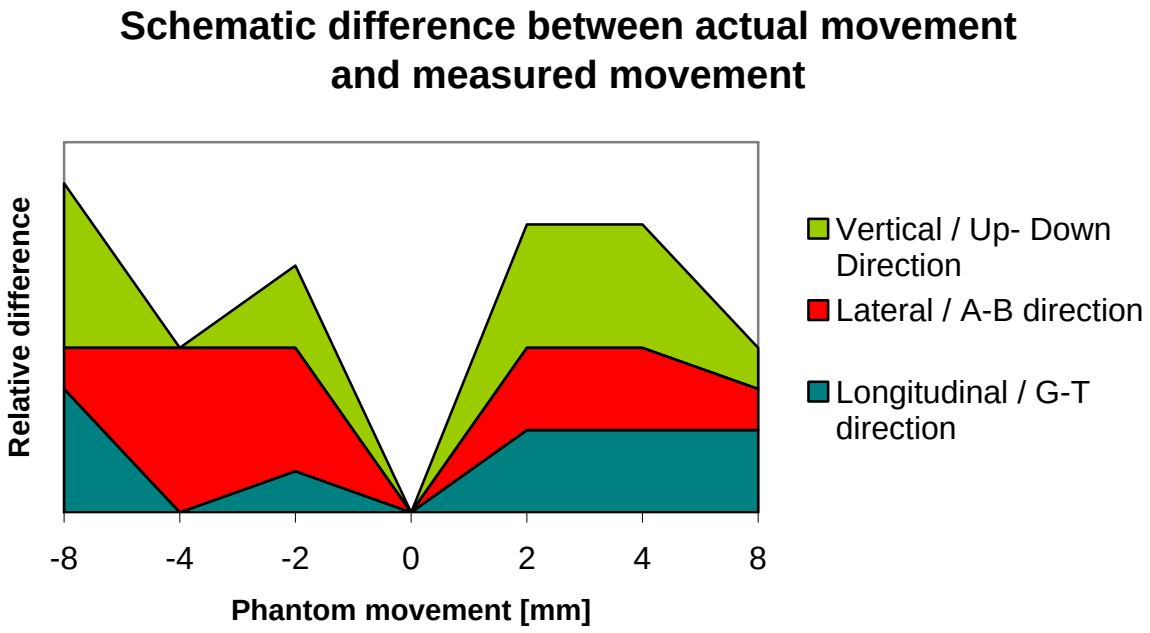

Figure 3.4 A schematic that shows the relative difference between laser and XVI given coordinates. The area for each colour gives a rough idea of how much the XVI coordinates in each of the linac directions diverge from laser coordinates.

When translation was made an equal distance in each of the three directions simultaneously, higher performance is demanded on the system. A logical theory in this case would be that setup detection errors in the software increase with increasing movement distances. The results of this measurement can be found in Table 3.3

Table 3.3 A summary of the deviation between the XVI software setup-errors and the laser movements when moving the phantom a specific length in all three directions. Phantom movement according to lasers are shown in bold text.

Direction A/G/Up				**Direction B/T/Down**			
	2mm	**4mm**	**8mm**		**2mm**	**4mm**	**8mm**
Lateral	0,1	0,2	0,5	Lateral	0,2	0,1	0,4
Longitudinal	0,0	0,4	0,3	Longitudinal	0,1	0,2	0,2
Vertical	0,5	0,3	0,2	Vertical	0,3	0,6	0,2

As can be seen, the results in Table 3.3 do not differ much from the results in Figure 3.3. A deviation of 0.5 mm in a 2 mm movement and a deviation of 0.6 mm in a 4 mm movement might seem quite large. It can be noted that both of these larger deviations are in the vertical direction of the movement. It must be kept in mind though that the reported errors include set-up errors of the phantom.

The last measurement in this study, when moving the phantom different lengths in all three directions showed similar results as in the other measurements. Altogether the XVI software seems very reliable in detecting setup-errors, even at submillimeter precision. This has been shown in several tests described in this section.

3.3.2 Alderson/Rando phantom study with inserted gold markers

The first scan of the Alderson/Rando phantom revealed that the isocenter in the treatment planned reference image was located 4 cm cranial of the prostate. Also, one of the gold markers was located to close to bony structure which resulted in problems to define a 3-D matching volume that did not contain any bony structures. Therefore attempts were made to make a matching with only two of the markers in the matching volume. When the button to initiate the matching procedure in the software was pushed nothing happened. It was still possible to do a greyscale matching. Given the problems described, a new measurement had to be done. In the new CT-scan, lead markers were placed at the laser crosses, which made it much easier to mark the isocenter in OMP. Also, one of the gold markers was moved to a location where it was not close to bone tissue. The imported images were then set as reference images in the XVI, using a matching volume that only contained the three gold markers. A new scan gave the result shown in Figure 3.5.

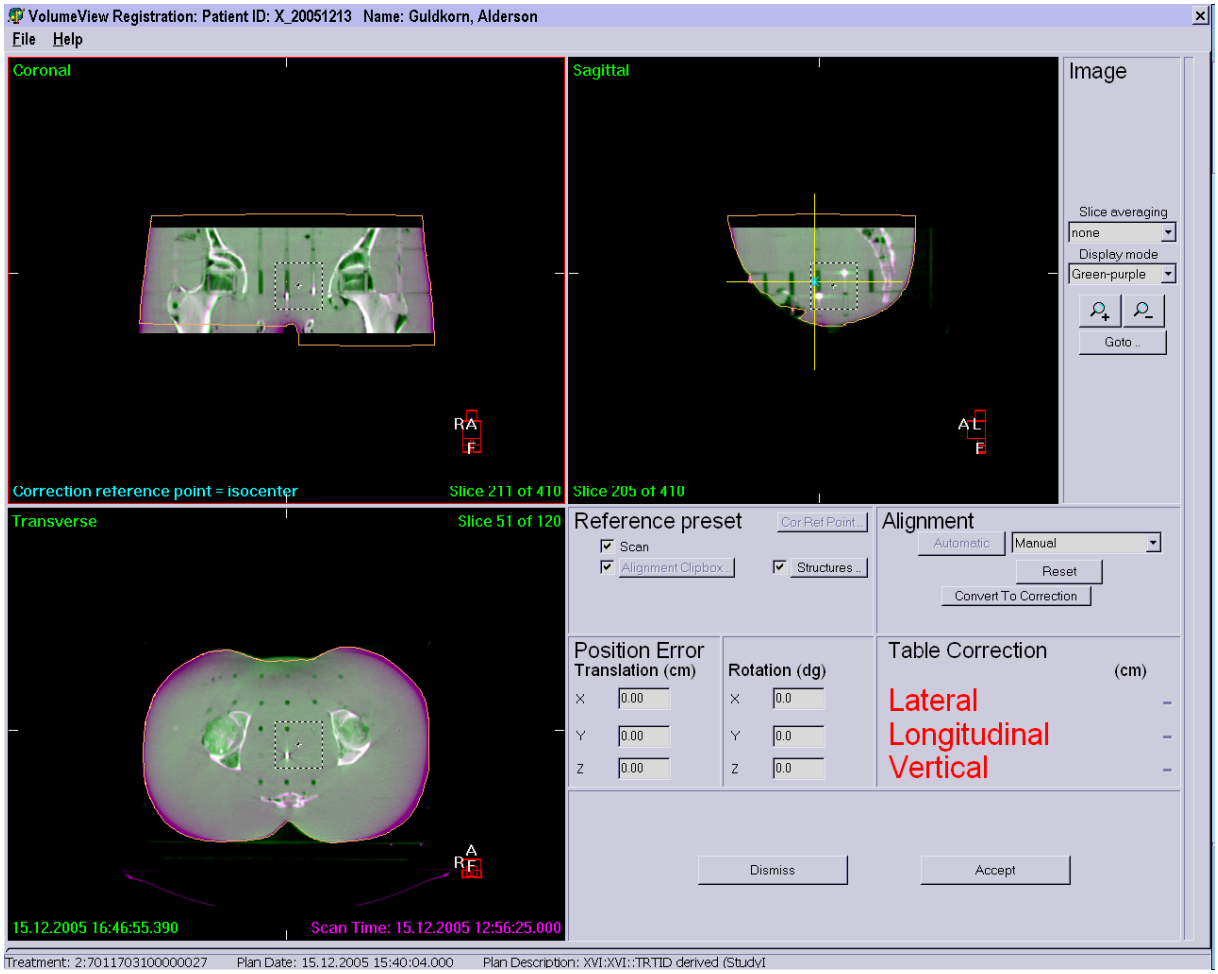

Figure 3.5 A screendump from the Alderson/Rando measurement with inserted gold markers. The matching volume is marked in each view by the dashed clickbox. It is shown that the gold markers, seen as bright dots, are contained within the box.

When trying to perform a match on the three gold markers alone we got the same results as in the first experiment, i.e. the software did not initiate a match. An assumption is that there was not enough high density material within the matching box, which resulted in that the software did not initiate the matching process. What contradicts this assumption is that in the case of a

real patient, it is possible to perform a match with a small matching volume confined by the gold markers. It could be the fact, that in a real clinical situation there is a larger amount of tissue that will be handled as “bony” tissue, and therefore the program is able to perform an automatic matching. Although, when trying to perform a matching using a too small matching volume with a real patient, an error message is displayed which explains that the clickbox do not contain enough bony tissue. The assumption on that this message was not received when trying to perform automatic matching in the Alderson/Rando phantom, is that those images were acquired in service mode instead of clinical mode. When reading the manual, reference [15, Appendix C2], about the Bone match algorithm (called Chamfer algorithm by Elekta) another explanation for the error occurs. A quote from the manual says:

“In some circumstances, it is possible that the chamfer algorithm will produce an incorrect registration solution, but not display any error message. These circumstances include:
• registration of spinal vertebrae: the algorithm may mis-register by one complete vertebra
• attempting to register mobile anatomy (e.g. neck)
• attempting to register image artefacts
• attempting to register the table top”

It does not seem like any of the explanations given above fits to my error search, but the possibility exists that one of the explanations mentioned causes the problem without me knowing about it.

A conclusion of the information given in this section is that it is not possible to make a three-dimensional automatic matching with only gold markers as a reference. Even if it is possible with real patients the results are not acceptable, unless the matching volume include bony tissues. This feature of the software can be regarded as inappropriate because the XVI unit was designed to better incorporate soft tissue matching.

3.4 X-ray tube performance

When examining output from the XVI both 100 kV and 120 kV was investigated. The mean values of three measurements for each defined kV are tabulated in Table 3.4.

Table 3.4 Measured parameters for the x-ray imaging tube. Total Filtration (TF) and Half Value Layer (HVL) show the amount of beam-hardening involved.

Defined kVp	Measured kVp	Irradiated time $[s]$	Dose $[\mu Gy]$	TF $[mm]$	HVL $[mm]$
100	103.7	2.94	169.0	7.3	5.1
120	125.4	2.94	270.1	7.0	5.9

Due to the increased photon fluence from the x-ray tube when increasing the tube voltage, kVp, we get a higher dose output at 120 kVp. The increased photon fluence arise from that more bremsstrahlung is created when electrons hit the target at higher energies [reference 20, p 209]. Tolerable deviation between measured and defined kVp is 5% for a modern x-ray source [14] and the Synergy is within these margins. The measured HVL on the other hand is well above the specification value of 3.6 mm in reference [18, section 3.3.1.1].

The dose linearity of the system showed almost perfect agreement with mAs. The results can be found in Figure 3.6.

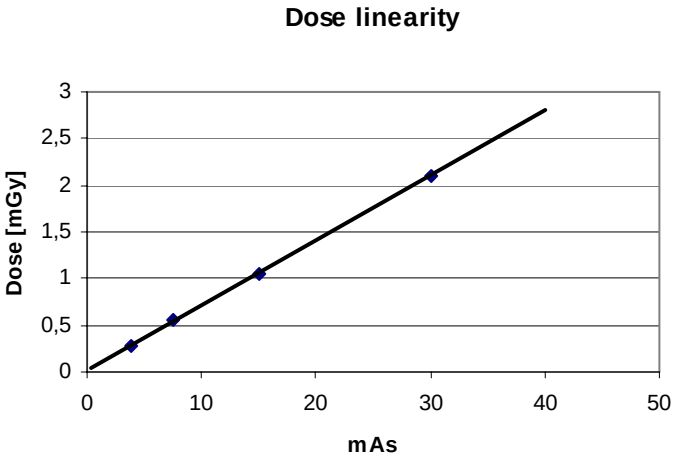

Figure 3.6 The dose output as a function of mAs from the X-ray tube.

3.5 X-ray imaging doses

3.5.1 CTDI

The XVI software displays that the dose received in a pelvis scan is approximately 16 mGy. A measurement according to Section 2.4.1 gives CTDI values as shown in Table 3.5.

Table 3.5 Calculated doses for pelvis scan using both a **M10** and a **M20** collimator. 120 kV and 650 mAs

Collimator	$CTDI_{100C}$ $[mGy]$	$CTDI_{100P}$ $[mGy]$	$CTDI_w$ $[mGy]$	$N \cdot d$ $[cm]$	DLP $[mSv \cdot cm]$	E_{DLP} $[mSv/(mGy \cdot cm)]$	Effective Dose $[mSv]$
M10	10.3	22.94	18.73	13.54	253.60	0.019	4.82
M20	12.62	24.46	20.51	27.67	567.51	0.019	10.78

Values for $N \cdot d$ is found in Table 3.5 and values for E_{DLP} are found in [13]

The dose tabulated in Table 3.5 describes the effective dose calculated with respect to the nominal irradiated length and weighted with the organ radiation sensitivity. Unfortunately in dosage aspects, the **M10** collimator does not give clinical usable images for a pelvis scan and that is why the preset suggest using an **M20** collimator instead. When imaging prostate it is preferable to use the narrower **M10** collimator. Therefore the tabulated effective dose, 4.82 mSv, in Table 3.5 gives a rough estimate of the dose received during a prostate scan.

Table 3.6 Calculated doses for a head-and-neck scan using a S20 collimator, 100 kV and 36.1 mAs

Treatment	$CTDI_{100C}$ $[mGy]$	$CTDI_{100P}$ $[mGy]$	$CTDI_w$ $[mGy]$	$N \cdot d$ $[cm]$	DLP $[mSv \cdot cm]$	E_{DLP} $[mSv/(mGy \cdot cm)]$	Effective Dose $[mSv]$
Head	1.04	1.26	1.19	27.67	32.87	0.0023	0.08
Neck	1.04	1.26	1.19	27.67	32.87	0.0054	0.18

Values for $N \cdot d$ is found Table 1.1 and values for E_{DLP} are found in [13]

The different effective doses for head and for neck arise from the specific E_{DLP} for head versus neck, respectively. As can be seen in Table 3.6 all CTDI and $N \cdot d$ are identical, which originates from that the values are from the same measurement and in the same geometry. The effective doses are relatively low compared to a pelvis scan, partly due to that the scan is made in half the rotation of a pelvis scan and partly because the preset uses lower kV and mAs (due to less attenuating material).

A similar measurement has been done on Christie Hospital in Manchester, UK. Their reported CTDI doses can be found in [9] and in [21]. In [21] they report that $CTDI_w$ for pelvis scans is approximately 25 mGy which is in good agreement with the 20.51 mGy found in this report. The same comparison with the head-and-neck phantom showed 1.2 mGy in this report and 1.6 mGy in the Christie Hospital report. The relatively small differences between both reports are probably due to uncertainties in the measurement but also to the fact that Christie Hospital used an earlier release of the machine.

3.5.2 TLD-doses

3.5.2.1 Pelvis

The result of the TLD measurement for the pelvis region is shown in Figure 3.7. It is apparent that the doses are higher near the edges of the phantom and decreasingly lower towards the centre of the phantom. This is because of the nonlinear depth dose curve across the phantom which is due to the attenuation of photons. In a circular scan this results in a decreasing absorbed dose towards the centre. In slices 31-32 the mean absorbed dose is 22.05 mGy and in slices 32-33 the mean absorbed dose is 20.68 mGy. The doses in the upper slices are slightly higher which probably depends on the increasingly amount of material that scatter radiation in the upper region. There was also one TLD placed between slices 25-26, which is located approximately 15 cm above slices 31-32. The irradiated length at isocenter using the **M20** collimator is 27.67 cm. The TLD placed between slices 25-26 is located exactly $15 + \frac{2.5}{2} = 16.25\,\text{cm}$ from the center of the beam and the beam stretches $\frac{27.76}{2} = 13.88\,\text{cm}$ in each direction. This means that the TLD is placed about 2.4 cm outside the beam. Still the dose to the TLD was 4.45 mGy, which probably arise from scattered radiation.

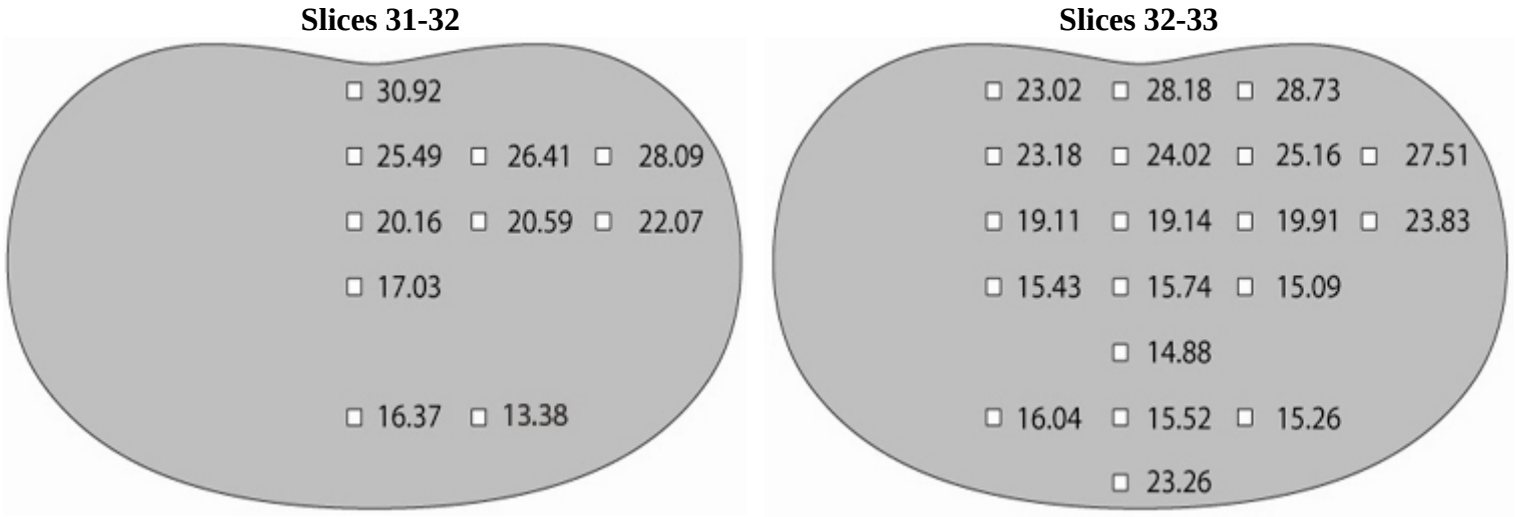

Figure 3.7 The position of the TLDs in the Alderson/Rando slices and their respective absorbed doses after a pelvis XVI scan. Slice 31-32 is located cranial of slice 32-33.

Again, the pelvis scan uses 120 kV and 650 mAs. The mean for both slices in Figure 3.7 is 21.37 mGy. A similar TLD-measurement has also been done by Christie Hospital, as mentioned in Section 3.5.1. They report a mean dose of 26 mGy [21] for a pelvis scan, with their x-ray tube using 130 kV and 458 mAs. Given that mAs and kV differed slightly between the two reports it is safe to say that both XVI units are quite similar regarding the dosimetric aspects.

3.5.2.2 Head and Neck

The x-ray beam covers all the inserted boards in the Alderson/Rando phantom. Slices 9-10 are located 10 cm beyond the center of slices 5-6 in the G-T direction, a distance that is within half the irradiated length at isocenter (half the irradiated length in each direction from isocenter accounts for the whole beam). This means that all TLDs are within the beam. The acquired doses to the TLDs, presented as figures that also explain the TLD positions, is illustrated in Figure 3.8.

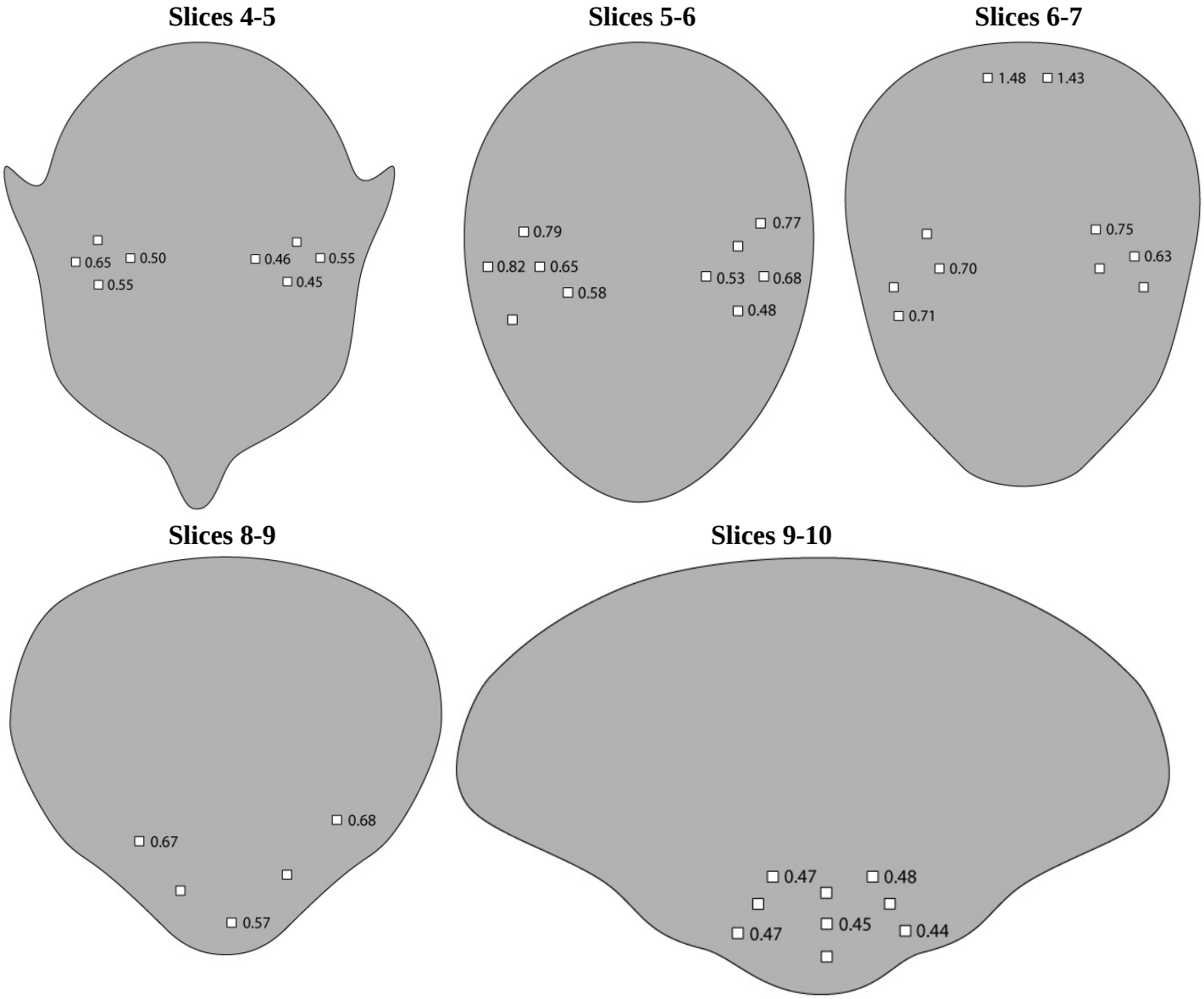

Figure 3.8 The doses from TLD-measurements in the head-and-neck slices of the Alderson/Rando phantom. All square holes with a number on the right side are filled with a TLD. Slice 4-5 is the most cranial slice and slice 9-10 is the most caudal.

Figure 3.8 shows that the absorbed doses are generally much lower compared to the pelvis scan. The major reasons for the lower absorbed doses are that the preset uses much less mAs and that the scan is made in a half-way rotation. Also, the preset uses 100 kV tube voltage instead of 120 kV as with a pelvis scan. The doses to each of the eyes are 0.37 mGy. Table 3.7 shows the mean dose in each slice.

Table 3.7 The mean absorbed dose in each slice of the Alderson/Rando phantom, head-and-neck region.

Slices	Mean dose in slices [mGy]
4-5	0.52
5-6	0.66
6-7	0.95
8-9	0.64
9-10	0.46

The highest absorbed mean dose were found at board 6-7 which was placed 2.5 cm caudal of the center of the beam. The higher dose in this slice originates from the two TLDs placed at the back of the head, which receive about twice the absorbed doses as all other TLDs. Table 3.7 shows that the mean absorbed dose from all slices is 0.65 mGy. Reference [9] reports a mean value of 0.95 mGy when using 100 kV and 30 mAs. The deviation from results in this work compared to [9] probably depends on different positioning of the TLDs. We used TLDs in between all six head slices of the Alderson Rando phantom, while Sykes, et al used only three slices. Also, shown in Figure 3.8, the distribution of TLDs in the back region (dorsal) may be insufficient. As the doses to the two dorsal TLDs in slices 6-7 is much higher than it is for other TLDs, it is assumed that the mean dose for all slices should actually be slightly higher. The mean absorbed dose in slice 6-7 is 0.95 mGy in this report, and that is exactly what Sykes, et al reports as the mean dose for their whole scan.

4. Conclusions and future work

Different aspects of the Elekta Synergy concept for patient positioning in IGRT have been evaluated. Because the Elekta concept is to have a kV imaging unit mounted on the radiotherapy unit, apart from the EPID device, my aim was to focus on XVI system. The first part of the thesis analyzed the flex in the gantry rotation during a three month period and the results showed only minor long term variations. If there had been a considerable flex it would have shown in the 3-D imaging tests. All but one of the 3-D imaging tests was acceptable during a three month period. The 3-D low contrast visibility seemed to have a trend to detoriate over time (Figure 3.2). As Elekta have promised to deal with this shortly we can summarize that the 3-D imaging is fully acceptable, including the flex of the gantry rotation. The 2-D imaging showed a low contrast visibility of 2.1% and a spatial resolution of 1.8 lp/mm. The spatial resolution in 3-D imaging was significantly lower but still sufficient, namely 0.7 lp/mm. Digital imaging with an ordinary x-ray examination unit shows a 2-D spatial resolution of about 5 lp/mm and the 3-D spatial resolution of an ordinary fan-beam CT unit is about 1 lp/mm [25], which shows that the XVI is inferior in both aspects. Elekta has noted in the manual [15] that the XVI is not supposed to be used for extensive diagnostic evaluations, but to minimize setup-errors upon treatment delivery.

This work also aimed to evaluate the clinical usage of the XVI imaging system for IGRT regarding correction of set-up errors. It has been shown in Section 3.3 that the system is very reliable in detecting setup-errors, at least if matching is performed on bony structures as in the case of the Pelvis phantom study. A maximum deviation between defined movement according to the lasers and the measured movement by an XVI scan was found to be 0.4 mm. This small deviation probably originates from our phantom set-up errors in relation to the lasers. The gold marker study described in Section 3.3.2 on the other hand showed that it is not possible to perform automatic “bone” matchings in the software with respect to the gold markers only. This could probably be corrected by a minor improvement of the software. Further on, the software should be improved so that soft tissue matching algorithms are available. The XVI software includes a “Greyscale” matching algorithm, but this algorithm ignores the matching volume defined by the “clickbox” and performs a matching based on greyscale values covering the complete image. It should also be mentioned that the “Greyscale” automatic matching algorithm has not been fully approved for clinical use by Elekta.

The results of Section 3.4 show that the output from the x-ray tube fulfils the requirements of a standard x-ray system.

Imaging doses from XVI scans were evaluated in Section 3.5, both by CTDI measurements and TLD measurements. It was shown that received effective doses, based on CTDI-measurements, were about 11 mSv for pelvis scans and about 0.15 mSv for head-and-neck scans. An ordinary CT examination in the pelvis region results in an effective dose of about 10 mSv [23,24] and ordinary CT scans in the head-and-neck region delivers about 1.5 mSv [24]. This means that the received dose in a pelvis scan is about the same for an XVI scan as for an ordinary CT scan. Regarding head-and-neck, the received effective dose for a XVI scan is about 1/10 times the received dose from an ordinary CT examination. The low dose for head-and-neck scans in the XVI probably arises from the fact that the preset uses low mAs (Table 3.6). The XVI scan is designed to correct setup errors according to the external structures of the head and on the cervical spinal cords, which justifies the implementation of a lower mAs.

Future work with the XVI could be to evaluate how well the system detects and corrects for patient setups that are rotated compared to the treatment planned CT-images. As described in this work only translational setup-errors have been studied and corrected for. Also it would be interesting to study the improvement of using kV 3D-images for detecting patient setup-errors compared to using only EPID-images. The results of such a study could also give information about in what cases 3D-imaging is needed and when it is sufficient to use orthogonal planar images. Also, additional work can be implemented in creating presets that are optimal for different examinations. For example, sufficient image quality may be achieved by using less projections or lower mAs, and that would spare absorbed doses given to the patient.

Appendix A. CTDI calculation

To calculate doses in conventional CT-scans the term CTDI, Computed Tomography Dose Index, is used. There are a lot of approximations in the definition but they are considered to be affordable. The definition of CTDI is the integral over the dose profile along a straight line parallel to the rotation axis, divided to the nominal slice thickness [13].

$$CTDI = \frac{1}{d}\int_{-a}^{+a} D(z)dz \qquad [\,mGy\,] \qquad (1)$$

where $D(z)$ is the air kerma rate and d is the nominal slice thickness.

The integration limits used are usually chosen as a 100 mm wide slice, because this is normally the active length of the ion chamber, which is placed in the CTDI phantom with the same width. The readouts from the ion chamber accounts for the $CTDI_{100}$ value. But the dose profile is not homogenous over each slice so a weighted value is which is approximated with the equation

$$CTDI_w = \frac{1}{3}CTDI_{100C} + \frac{2}{3}CTDI_{100P} \qquad (mGy) \qquad (2)$$

where $CTDI_{100C}$ is measured in the centre of the phantom and $CTDI_{100P}$ is a mean dose of four different CTDI-values measured in the periphery of the phantom. Equation (2) follows from the assumption that the dose decreases in radial direction from the center of the phantom [23].

The Dose Length Product, *DLP*, is then calculated using the equation

$$DLP = N \cdot d \cdot CTDI_w \qquad (mGy \cdot cm) \qquad (3)$$

where N is the number of rotations around the axis and d is the slice thickness. These equations are used for the conventional CT-scanner. If imaging with the XVI, when cone beam CT is used, there is no slice thickness or number of rotations in Equation (3). Instead the irradiated length at isocenter is employed, and those values can be found in Table 1.1. The effective dose for a specific anatomic area can then be calculated according to the formula

$$E = E_{DLP} \cdot DLP \qquad (mSv) \qquad (4)$$

Where E_{DLP} is given in $\left[\frac{mSv}{mGy \cdot cm}\right]$ and varies with different anatomical areas. E_{DLP} can be found in [13]. Note that these values are calculated for a conventional CT-scanner which uses fan-beam technology. It is a slight approximation when using these E_{DLP}-values for cone-beam scans.

Acknowledgements

I would like to thank many friends and colleagues who have helped me with this thesis. First I like to thank my supervisors Per Nilsson and Tommy Knöös who generously have sacrificed time to my aid in their busy schedules. I also owe enormous dept of gratitude to Sonny La who have supported me in several measurements, when I still was unfamiliar to the preface of the radiotherapy unit. He also helped me perform ordinary CT scans prior to treatment planning. For the treatment planning I am in dept to Petra Ambolt, while she helped me adding fields in OMP and exported the DICOM images to the XVI.

I am also deeply indebted to Inga Göransson who patiently showed me how to handle TLD's and also helped me with the TLD readouts. I would also like to thank Gunnila Holje who has answered questions regarding the x-ray measurements and provided me with equipment needed to implement them.

I acknowledge with gratitude the help from Andrej Tomaszewicz who mainly have aided me in the gold marker study but also have answered general questions about the XVI system. In the detection limit study, Medical Physics student Jonathan Siikanen helped me to perform the measurement, and for that I am very grateful. Also, I would like to thank the staff at the workshop for providing me with the equipment needed for both of the detection limit studies.

Finally, I thank my girlfriend, Åsa Jansson, who is the designer of several illustrations seen in this work and also the layout advisor of both the report and the PowerPoint presentation of my work. She also has been a great encouragement when I needed it most.

Thanks!

References

1. David A. Jaffray. Emergent Technologies for 3-Dimensional Image-Guided Radiation Delivery. Semin Radiat Oncol 15:208-216
2. David A. Jaffray, Jeffrey H. Siewerdsen, John W. Wong, Alvaro A. Martinez. Flat-panel cone-beam computed tomography for image-guided radiation therapy. Int. J. Radiation Oncology Biol. Phys., Vol 53. No. 5 pp. 1337-1349, 2002
3. Jean Pouliot, Ali Bani-Hashemi, Josephine Chen, et al. Low-dose megavoltage cone-beam CT for radiation therapy. Int. J. Radiation Oncology Biol. Phys., Vol 61. No. 2 pp. 552-560, 2005
4. Daniel Létourneau, John W. Wong, Mark Oldham, et al. Cone-beam-CT guided radiation therapy: technical implementation. Radiotherapy and Oncology 75 (2005) 279-286
5. Mark Oldham, Daniel Létourneau, Lindsay Watt, et al. Cone-beam-CT guided radiation therapy: A model for on-line application. Radiotherapy and Oncology 75 (2005) 271.e1-271.e8
6. L. A. Feldkamp, L. C. Davis, J. W. Kress. Practical cone-beam algorithm. J. Opt. Soc. Am. A/Vol. 1, No. 6/June 1984
7. Q Huang, G L Zeng, J You, G T Gullberg. An FDK-like cone-beam SPECT reconstruction algorithm for non-uniform attenuated projections acquired using a circular trajectory. Phys.Med. Biol. 50 (2005) 2329-2339
8. Lifeng Yu, Xiaochuan Pan, Charles A. Pelizzari. Image Reconstruction with a Shift-Variant Filtration in Circular Cone-Beam CT. Int J Imaging Syst Technol, 14, 213-221, 2004
9. Jonathan R. Sykes, Ali Amer, Jadwiga Czajka, Christopher J. Moore. A feasibility study for image guided radiotherapy using low dose, high speed, cone beam X-ray volumetric imaging. Radiotherapy and Oncology 77 (2005) 45-52
10. Paul S Cho, Roger H Johnson, Thomas W Griffin. Cone-beam CT for radiotherapy applications. Phys. Med. Biol. 40 (1995) 1863-1883
11. P Sukovic. Cone beam computed tomography in craniofacial imaging. Orthod. Craniofacial Res. 6 (Suppl. 1), 2003; 31-36
12. Ali Amer, Jonathan Sykes, Christopher Moore. Imaging Panel Skew Correction and Auto-focusing in Radiotherapy Cone Beam Imaging. Proceedings of the Eighth International Conference on Information Visualisation (IV'04) 1093-9547/04
13. Statens strålskyddsinstitut SSI, Kommentarer till Statens strålskyddsinstituts föreskrifter och allmänna råd (SSI FS 2002:2) om diagnostiska standarddoser och referensnivåer inom röntgendiagnostiken
14. SSI FS 1995:1, Statens strålskyddsinstituts allmänna råd om prestandaspecifikationer vid upphandling av utrustning för röntgendiagnostik
15. Elekta. Clinical User Manual for XVI R3.5. Document number 4513 370 2170 01
16. Elekta. Customer Acceptance Tests for XVI R3.5. Document number 4513 370 2139 01
17. Elekta. Installation Manual for XVI R3.5,
18. Elekta. Elekta Synergy Corrective Maintenance Manual for XVI
19. The Phantom Laboratory, Catphan® 500 and 600 Manual
20. Frank H. Attix, Introduction to radiological physics and radiation dosimetry
21. Elekta European Users Conference, Madeira, June '05.
22. Henrik Turbell. Cone-Beam Reconstruction Using Filtered Backprojection. Linköping Studies in Science and Technology, Dissertation No. 672

23. H. Imhof, N.Schibany, A. Ba-Ssalamah. Spiral CT and radiation dose. European Journal of Radiology. 47 (2003) 29-37
24. P. C Shrimpton, M. C Hillier, M. A Lewis, M Dunn. Doses from Computed Tomography (CT) Examinations in UK – 2003 Review. NRPB – W67 (2005)

Image and web references

25. Lecture about medical imaging given in Dartmouth, available at: http://thayer.dartmouth.edu/~bpogue/ENGG167/14%20Computed%20Tomography.pdf, [verified: 060224]
26. Brainlab, Brochure about ExacTrac® X-Ray 6D, available at: http://www.brainlab.com/download/pdf/IGTExacTracBrochure.pdf [verified: 060224]
27. Innsbruck Medical University, Aldersson/Rando image, available at: http://www.uibk.ac.at/c/c5/c502/images/ossi1.gif [verified: 060224]